UMEÅ UNIVERSITY

^{11}C-Acetate-PET/CT in Primary Staging of High-Risk Prostate Cancer

Sara Strandberg

Department of Radiation Sciences
Umeå 2020

Dissertation for PhD
ISBN (Printed): 978-91-7855-206-1
ISBN (Digital): 978-91-7855-207-8
ISSN 0346-6612
UMEÅ UNIVERSITY MEDICAL DISSERTATION
New Series Number 2072
Cover photo by Karin Berlin: “The road forward, in hot iron color scale”, Öland East coast
Electronic version available at: http://umu.diva-portal.org/
Printed by: CityPrint i Norr AB
Umeå, Sweden 2020

In memory of my grandfather Ove Alexander Lengström (1919-2010).

Table of Contents

Abstract

Prostate cancer (PC) is the second most common cancer in men worldwide, affecting ~12%. Although most are clinically insignificant low-risk cancers, the more aggressive high-risk cancers require correct staging, prior to curative radiotherapy or surgery. Standard staging procedures and tools include clinical examination, estimated nomogram risk of pelvic lymph node (LN) metastases, and bone scintigraphy (BS). Additional staging information can be obtained with magnetic resonance imaging (MRI), computed tomography (CT) and positron-emission tomography/computed tomography (PET/CT). PET/CT can provide information on both functional and morphological changes.
The aims of the present thesis were to investigate the diagnostic and prognostic value of ^{11}C-acetate (ACE)-PET/CT in high-risk PC, and to optimize the ACE-PET protocol. In study I and II, higher detection rates of LN metastases and bone metastases were found with ACE-PET/CT, than with standard methods nomogram risk and BS. The higher ACE uptake in the prostate (prostate lipogenic tumor burden), the higher the risk of suspected LN metastases (N+ disease) on PET/CT. ACE-PET/CT findings correlated better than BS with follow-up data, and influenced therapy in 11-43%. In study III, PET reconstruction algorithm with resolution recovery showed more accurate functional tumor volumes compared to CT, and higher measurements of lipogenic activity, than reconstruction algorithm without resolution recovery. Study IV was part of an interventional radiotherapy study (PARAPLY) on high-risk PC, with addition of image-guided simultaneous integrated boost to delineated prostate tumors and pelvic LN metastases reported in ACE-PET/CT and MRI. Comparative analyses of clinical risk parameters and baseline ACE-PET/CT parameters showed significant associations between nomogram risk and prostate lipogenic tumor burden, between N+ disease on PET/CT and prostate lipogenic tumor burden, but surprisingly not between nomogram risk and N+ disease on PET/CT. PET with resolution recovery was superior in detection of N+ disease.
In conclusion, ACE-PET/CT showed a higher detection rate of suspected metastases compared to standard methods clinical nomogram and BS, in high-risk PC. PET reconstruction with resolution recovery seems to improve the diagnostic added value of ACE-PET/CT. Prostate lipogenic tumor burden could serve as a predictor of N+ disease. The prognostic value of ACE-PET/CT remains to be investigated in future studies.

Abbreviations

ACE	^{11}C-acetate
BS	bone scintigraphy
CoA	coenzyme A
CT	computed tomography
DIL	dominant intra-prostatic lesion
EAU	European Association of Urology
FDG	^{18}F-2-deoxy-2-[^{18}F]-D- glucose
FTV	functional tumor volume
GS	Gleason score
HDP	hydroxymethylene diphosphonate
IR	iterative reconstruction
ISUP	International Society of Urological Pathology
keV	kiloelectronvolt
LN	lymph node
mpMRI	multiparametric magnetic resonance imaging
MRI	magnetic resonance imaging
N+	presence of pelvic lymph node metastases
OSEM	ordered subsets expectation maximization
PC	prostate cancer
PET/CT	positron-emission tomography/computed tomography
PSA	prostate-specific antigen
PSMA	prostate-specific membrane antigen
RC	recovery coefficient
S/B	signal-to-background
SharpIR	VUEPointHD™ SharpIR
SPECT	single photon emission computed tomography
SPECT/CT	single photon emission computed tomography/computed tomography
SUV_{max}	maximum standardized uptake value
$SUV_{max,DIL}$	SUV_{max} of the DIL
$SUV_{max,LN}$	highest SUV_{max} of the LNs
SUV_{mean}	mean standardized uptake value
TLG	total lesion glycolysis
TLU	total lipogenic uptake
TNM	Tumor Node Metastasis
VPHD	VUEPointHD™ ViP

Sammanfattning på svenska

^{11}C-acetat-PET/CT vid primär stadieindelning av prostatacancer av högrisktyp

Prostatacancer är den näst vanligaste cancersjukdomen hos män sett ur ett globalt perspektiv, ca 12% drabbas under sin livstid. De flesta prostatacancertumörerna är av klinisk lågrisktyp med stillsamt förlopp, men det finns också betydligt mer aggressiva former. Dessa högrisktumörer kan behandlas kurativt med strålbehandling eller kirurgi, men detta förutsätter korrekt stadieindelning enligt TNM-klassifikationen (T - primär tumörutbredning, N - lymfkörtelmetastasering, M - fjärrmetastasering).
Standardmetod för bedömning av T-stadium är rektalpalpation. För uppskattning av N-stadium beräknas risk för lymfkörtelmetastasering i kliniskt nomogram, utifrån riskfaktorer som ålder, prostata-specifikt antigen (PSA) och Gleason score. Då prostatacancer ofta metastaserar till skelettet används skelettscintigrafi i stor utsträckning för bedömning av M-stadium.
Magnetresonanstomografi (MR), datortomografi (computed tomography, CT) och positronemissionstomografi kombinerad med datortomografi (PET/CT) kan bidra med ytterligare information av värde för stadieindelningen. PET/CT kan påvisa både funktionella (PET) och morfologiska (CT) förändringar.
Denna avhandling syftar till att utvärdera det diagnostiska och prognostiska värdet av ^{11}C-acetat (ACE)-PET/CT vid primär stadieindelning av prostatacancer av högrisktyp, samt att optimera undersökningsprotokollet för ACE-PET.
I studie I och II uppvisade ACE-PET/CT högre detektionsgrad av suspekta lymfkörtel- och skelettmetastaser än standardmetoderna kliniskt nomogram respektive skelettscintigrafi. Ju högre ACE-upptag i prostata (lipogen tumörbörda i prostata), desto större var risken för misstänkt lymfkörtelmetastasering (N+ sjukdom) på PET/CT. Fynden vid ACE-PET/CT korrelerade bättre än skelettscintigrafi mot uppföljningdata. ACE-PET/CT påverkade handläggningen av patienterna i 11-43%. I studie III identifierades förbättringsområden avseende PET-rekonstruktionsalgoritm. Rekonstruktion med bättre upplösning (resolution recovery) gav mer korrekta funktionella tumörvolymer, med

strukturell CT-volym som referens, och högre värden på lipogen aktivitet, än standardrekonstruktion.
Studie IV baserades på baseline-data från PARAPLY-studien, en interventionsstudie på prostatacancer av högrisktyp, där primärtumören och eventuella lymfkörtelmetastaser utlinjeras med hjälp av ACE-PET/CT och MR, och behandlas med lokalt utökad strålbehandling (simultaneous integrated boost) utöver standardstrålfält. Jämförande analyser mellan kliniska riskparametrar och ACE-PET/CT-parametrar visade signifikant samband mellan nomogramrisk och lipogen tumörbörda i prostata, men överraskande nog inte mellan nomogramrisk och N+ sjukdom på PET/CT. Sambandet som påvisades i studie I mellan lipogen tumörbörda i prostata och N+ sjukdom på PET/CT kunde dock bekräftas. Med PET-rekonstruktion med resolution recovery hittades fler patienter med N+ sjukdom.
Sammanfattningsvis påvisades ett diagnostiskt tilläggsvärde av ACE-PET/CT, styrkt av begränsat uppföljningsdata, jämfört med standardmetoder kliniskt nomogram och skelettscintigrafi, vid primär stadieindelning av prostatacancer av högrisktyp. PET-rekonstruktion med resolution recovery förefaller öka det diagnostiska tilläggsvärdet av ACE-PET/CT. Lipogen tumörbörda i prostata kan vara en prediktor för N+ sjukdom. Det prognostiska värdet av ACE-PET/CT vid prostatacancer av högrisktyp kommer att utvärderas i kommande studier inom ramen för PARAPLY-studien.

List of papers

This thesis is based on the following three publications in peer-reviewed journals, and one manuscript, which are referred to in the text by their Roman numerals.

I. Strandberg S, Karlsson C, Sundström T, Ögren M[1], Ögren M[2], Axelsson J, Riklund K. ^{11}C-acetate PET/CT in pre-therapeutic lymph node staging in high-risk prostate cancer patients and its influence on disease management - a retrospective study. EJNMMI Res. 2014 Dec;4(1):55. DOI: 10.1186/s13550-014-0055-1.

II. Strandberg S, Karlsson C, Ögren M[1], Axelsson J, Riklund K. ^{11}C-acetate-PET/CT compared to ^{99m}Tc-HDP bone scintigraphy in primary staging of high-risk prostate cancer. Anticancer Res. 2016 Dec;36(12):6475-6479. DOI: 10.21873/anticanres.11246.

III. Strandberg S, Hashemi A, Axelsson J, Riklund K. Optimization of PET reconstruction algorithm, SUV thresholding algorithm and PET acquisition time in clinical ^{11}C-acetate PET/CT. PLOS ONE. 2018 Dec; 13(12): e0209169. DOI: 10.1371/journal.pone.0209169.

IV. Strandberg S, Karlsson C, Axelsson J, Riklund K. Baseline ^{11}C-acetate-PET/CT-derived parameters compared with clinical pre-treatment risk parameters in primary staging of high-risk prostate cancer – possible prognostic implications.
Manuscript.

Reprints were made with kind permission from the respective publishers.

Introduction

Epidemiology of prostate cancer

Approximately 12% of all men will be diagnosed with prostate cancer (PC), the second most common cancer in males globally (1). According to the Swedish National Prostate Cancer Registry, PC is the most common cancer in males in Sweden, with an incidence of 10000 cases and a mortality rate of 2500 cases per year (2).
The aetiology and pathogenesis of PC remain unclear, although it has been suggested in epidemiologic studies that systemic metabolic disorders including obesity, metabolic syndrome and type 2 diabetes, and dietary fat might increase the risk of PC (3). There is also growing evidence for the existence of a hereditary form of PC, with early-age onset and aggressive natural course (4).
PC is a heterogeneous malignancy, where most tumors are clinically insignificant low-risk cancers (5). Of all patients diagnosed with PC, 77% have localized PC and 13% have regional lymph node (LN) metastases at the time of diagnosis, with 100% 5-year-survival in both groups (1). However, the more aggressive high-risk forms of PC have poor prognosis; 6% of all PCs present with distant metastases, with a 5-year-survival of only 30% (1).

Clinical settings and treatments of prostate cancer

Given the broad spectrum of PCs and the long-term survival statistics, many different clinical settings of PC are encountered. In low-risk PC,

active surveillance is usually recommended, which means regular monitoring but no treatment unless there is sign of progression.
Curative treatment options for intermediate- and high-risk PC without distant metastases, consist of radical prostatectomy with optional pelvic LN dissection, or radiotherapy. Standard external-beam radiotherapy includes the prostate and the seminal vesicles (78 Gy) (6). A more targeted, imaging-guided radiotherapy approach is under development, where optional dose escalation, simultaneous integrated boost, is given to the dominant intra-prostatic lesion (DIL) and suspected pelvic LN metastases, in addition to standard radiotherapy (6). External radiotherapy can be combined with internal radiotherapy, brachytherapy, in which radionuclides constitute the source of radiation.
Another treatment option for high-risk PC is androgen deprivation therapy, which is achieved through chemical or surgical castration. Androgen deprivation therapy will inhibit PC growth, since most PCs are hormone (testosterone)-dependent initially, but will not cure the patient. Androgen deprivation therapy is used for high-risk PC with distant metastases, or as neoadjuvant or adjuvant therapy in patients receiving curative radiotherapy. In case of recurrence despite curative treatment, biochemical relapse is defined as a rise in prostate-specific antigen (PSA) >0.1-0.4 ng/mL after radical prostatectomy (7,8), or >2 ng/mL after radiotherapy (9).

Eventually, all PCs will become hormone-independent and enter the stage of castration-resistant PC, due to tumor mutations. In castration-resistant PC, residual intratumoral and intraadrenal androgen levels remain high, thereby making it possible to pharmaceutically target the

androgen axis from another angle. Such anti-androgen drugs are either androgen biosynthesis inhibitors (e.g. abiraterone) or androgen receptor blockers (e.g. enzalutamide) (10). In advanced metastatic castration-resistant PC, and possibly at earlier stages, addition of chemotherapy with docetaxel can be considered (11).

Anatomical aspects of prostate cancer

The prostate is a male reproductive androgen-regulated organ. Its main function is the secretion of an alkaline component of the semen which is vital for sperm cell function. The prostate consists of the peripheral zone, the central zone, the transitional zone, the periurethral tissue and the anterior fibromuscular tissue. Schematic illustrations of prostate anatomy are shown in figure 1 (12).

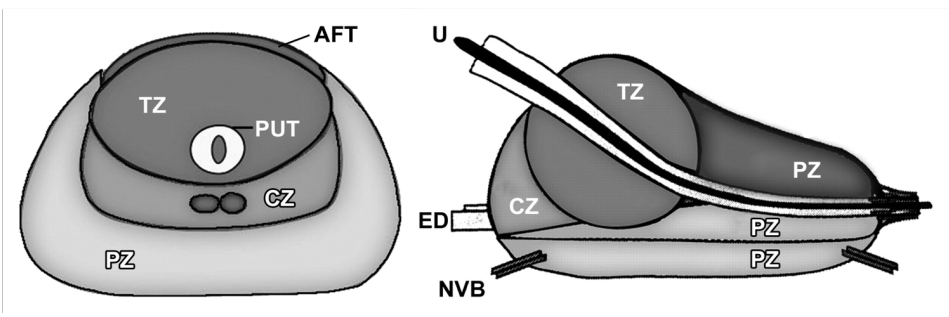

Figure 1. Prostate anatomy in transverse (left) and sagittal (right) planes. AFT anterior fibromuscular tissue, CZ central zone, ED ejaculatory duct, NVB neurovascular bundle, PUT periurethral tissue, PZ peripheral zone, U urethra, TZ transitional zone. Image reprinted from Choi YJ et al. Functional MR imaging of prostate cancer. RadioGraphics 2007; 27: 63-77, with kind permission from the Radiological Society of North America.

Most PCs (70-75%) occur in the peripheral zone. 20-30% of PCs arise in the transitional zone, which also is the site for benign prostatic hyperplasia. Merely 0-5% of PCs are reported in the central zone, however it is unclear whether these PCs possibly originate from the peripheral zone with subsequent invasion of the central zone. PC rarely arises in the anterior fibromuscular tissue and the periurethral tissue (12).

Prostate biopsies

In patients with suspected PC, systematic prostate biopsies are performed via transrectal or transperineal approach. The Swedish national biopsy template is illustrated in figure 2.

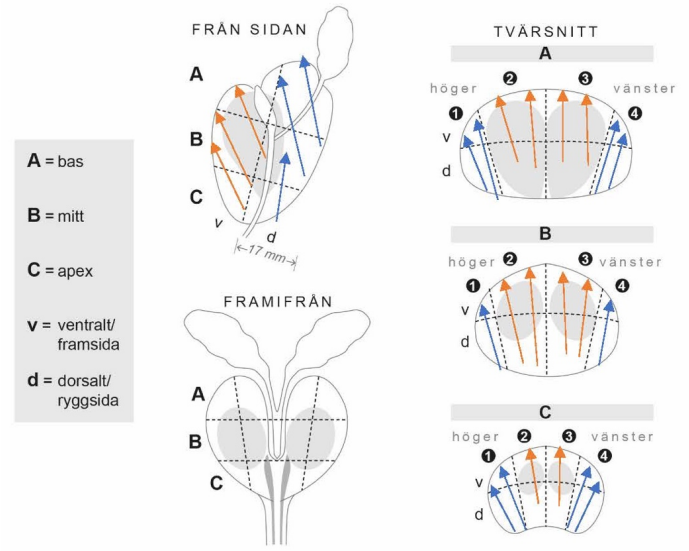

Figure 2. Swedish national template for localization of systematic transrectal ultrasound-guided prostate biopsies. 8-12 biopsies are routinely performed. Image reprinted from https://www.cancercentrum.se/samverkan/cancerdiagnoser/prostata/vardprogram/gallande-vardprogram-prostatacancer/9.-diagnostik, with kind permission from Regionala cancercentrum i samverkan and Sveriges Kommuner och Regioner.

In a registry study of comparative survival of histopathological subtypes in PC, over 99% consisted of conventional adenocarcinoma (13). The remaining variants were ductal carcinoma, mucinous adenocarcinoma, small cell carcinoma, carcinosarcoma and embryonal carcinosarcoma. Except for poorer survival in small cell carcinoma and carcinosarcoma, survival did not differ between the histopathological subtypes (13).

Ductal carcinoma, small cell carcinoma and both types of carcinosarcoma showed a higher frequency of metastases (13).

Risk categorization

Risk categorization of PC is based on clinical and histopathological features, mainly T stage, PSA and Gleason score (GS). Clinical examination of the prostate by digital rectal exam and transrectal ultrasound, provides information about the local tumor extent, or the clinical T stage.
Staging of PC according to the 2017 Tumor Node Metastasis (TNM) classification is shown in figure 3 (14).

T - Primary Tumour (stage based on digital rectal examination [DRE] only)		
TX	Primary tumour cannot be assessed	
T0	No evidence of primary tumour	
T1	Clinically inapparent tumour that is not palpable	
	T1a	Tumour incidental histological finding in 5% or less of tissue resected
	T1b	Tumour incidental histological finding in more than 5% of tissue resected
	T1c	Tumour identified by needle biopsy (e.g. because of elevated prostate-specific antigen [PSA])
T2	Tumour that is palpable and confined within the prostate	
	T2a	Tumour involves one half of one lobe or less
	T2b	Tumour involves more than half of one lobe, but not both lobes
	T2c	Tumour involves both lobes
T3	Tumour extends through the prostatic capsule	
	T3a	Extracapsular extension (unilateral or bilateral)
	T3b	Tumour invades seminal vesicle(s)
T4	Tumour is fixed or invades adjacent structures other than seminal vesicles: external sphincter, rectum, levator muscles, and/or pelvic wall	
N - Regional (pelvic) Lymph Nodes[1]		
NX	Regional lymph nodes cannot be assessed	
N0	No regional lymph node metastasis	
N1	Regional lymph node metastasis	
M - Distant Metastasis[2]		
M0	No distant metastasis	
M1	Distant metastasis	

Figure 3. The 2017 TNM classification of PC.

The Gleason grading system is a histopathological pattern scale, where 1-2 resemble normal prostate tissue, and are not used in the context of PC. Gleason grade 3-5 represent increasingly dedifferentiated, or anaplastic, cancer. GS is the sum of the most common Gleason grade and the next most common Gleason grade in the biopsied tissue samples. GS ranges from 2 to 10, the higher the score, the worse the prognosis. The GS system is continuously upgraded; the latest modification is the 2014

International Society of Urological Pathology (ISUP) endorsed grading system, ranging from 1-5, with ISUP grade increasing with GS (15). PC is categorized into low-, intermediate- and high-risk, according to different risk stratification systems (16). The European Association of Urology (EAU) risk stratification for recurrence of PC is illustrated in table 1 (10).

Low-risk	**Intermediate-risk**	**High-risk**
PSA <10 ng/mL AND	PSA 10-20 ng/mL OR	PSA >20 ng/mL OR
GS<7 AND	GS = 7 OR	GS>7 OR
cT1-2a	cT2b	cT3-4 / cN+[1]

Table 1. EAU risk stratification for recurrence of PC.

Clinical pre-treatment prediction nomograms are used to estimate the risk of suspected pelvic LN metastases (N+ disease). The clinical nomogram is an established prognostic tool based on clinical parameters, e.g. PSA, GS, age and number of positive prostate biopsy cores (17), where >15% estimated risk of N+ disease qualifies as high-risk PC. Nomograms will however only provide an estimated statistical risk of N+ disease, and to personalize treatment and target specific lesions, a more reliable method for individual PC staging is required.

[1] cN+ - clinically suspected pelvic LN metastases.

Metastatic pathways and sites of predilection

To improve staging, it is vital to understand the mechanisms behind PC tumor spread. The first sites of metastatic spread in PC are pelvic LNs, paraaortal LNs and bone (18). Typical locations of pelvic LN metastases are the external iliac region/obturator fossa, internal iliac, common iliac and distal paraaortal regions, listed in decreasing frequency (19). The lymphatic drainage pattern in PC does not convincingly adhere to the concept of sentinel node, where a tumor-free sentinel node implies that the following LNs along the same drainage route will be tumor-free as well. Results from peroperative sentinel node detection during extended pelvic LN dissection show a large variation in sentinel node localization (20). Sentinel nodes were found mainly in the expected external and internal iliac regions, but also in the common iliac and distal paraaortal regions (20). Surprisingly, sentinel nodes could also be localized in contralateral pelvic LNs (20). In autopsy material, simultaneous hematogeneous dissemination was markedly more frequent in PCs with paraaortal LN metastases than in those with pelvic LN metastases only (18).

Bone metastases occur early in the metastatic process (18). The underlying molecular mechanisms for the PC osteotropism are not yet fully understood (21). Except for bone, distant metastases may be found in lungs, liver, pleura, kidneys and adrenals (22). In autopsy material, metastases could be found in almost any organ (18). PC metastases in such rare sites most frequently occur in the setting of widely disseminated bone and soft tissue disease.

Hallmarks of cancer and de novo lipogenesis in prostate cancer

According to the paradigm of "Hallmarks of cancer" as proposed by Hanahan and Weinberg (23,24), cancer development in general is dependent on a number of fundamental features. These suggested hallmark traits include sustaining proliferative signaling, evading growth suppressors, resisting programmed cell death (apoptosis), enabling replicative immortality, inducing angiogenesis, reprogramming of energy metabolism, evading immune destruction, and activating tissue invasion and metastasis (figures 4a and b). Genome instability and inflammation provide the foundation for the development and maintenance of these hallmarks.

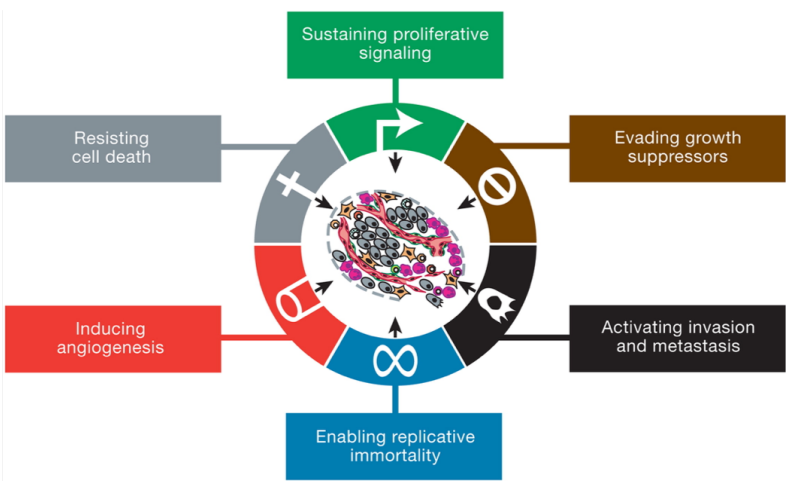

Figure 4a. Hallmarks of cancer. Image reprinted from Douglas Hanahan and Robert A. Weinberg. Hallmarks of Cancer: The Next Generation. Cell 2011; 144, March 4: 646-674, with kind permission from Elsevier Inc.

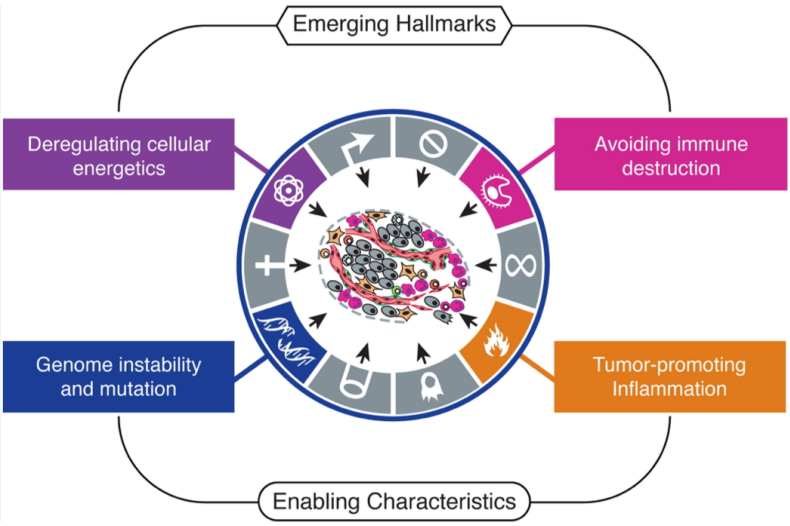

Figure 4b. Emerging hallmarks of cancer. Image reprinted from Douglas Hanahan and Robert A. Weinberg. Hallmarks of Cancer: The Next Generation. Cell 2011; 144, March 4: 646-674, with kind permission from Elsevier Inc.

In addition, tumors engage apparently normal cells within the tumor, to establish and maintain a suitable tumor microenvironment (24). This tumor signaling is also used in interaction with distant sites, such as bone marrow and lymphatic vessels, to create pre-metastatic niches for future metastatic tumor cells (25,26).

In PC, as in many other cancers, the hallmarks of maintaining proliferative signaling and resisting programmed cell death, are fulfilled. In the normal prostate epithelium, there is a balance between the rate of cell proliferation and the rate of apoptosis, while in PC, this balance is disrupted (27).

Another more distinguishing feature of PC, is the reprogramming into lipid energy metabolism. Normal prostate cells utilize glucose oxidation to provide precursors for the synthesis and secretion of citrate, resulting

in an incomplete Krebs cycle and minimal oxidative phosphorylation for energy production (3). During PC carcinogenesis, the cancer cells no longer secrete citrate, but instead reactivate the Krebs cycle and switch to lipid metabolism with increased de novo lipid synthesis (3). In PC, the cancer hallmark of reprogramming of cellular energy metabolism, is thus represented by the up-regulation of lipogenic enzymes (including fatty acid synthase and choline kinase) (3,28,29). Altered lipid metabolism plays a crucial role in the development and progression of PC, and correlates with worse prognosis and poor survival (3,28,29). It has been shown that de novo lipogenesis is essential for PC, thereby enabling a possible diagnostic target (30).

Based on this knowledge, lipid precursors such as acetate and choline have been introduced as radiotracers, ^{11}C-acetate (ACE) and ^{11}C-/^{18}F-choline, for PC imaging with positron-emission tomography/computed tomography (PET/CT). PCs do not show increased aerobic glycolysis and are therefore not suitable for ^{18}F-2-deoxy-2-[^{18}F]-D- glucose (FDG) - PET/CT (3).

Medical imaging in prostate cancer

Several imaging modalities are used for staging of PC. Radiological imaging such as computed tomography (CT) and multi- or biparametric magnetic resonance imaging (MRI), nuclear medicine imaging such as bone scintigraphy (BS), and hybrid imaging such as PET/CT, are common methods with different diagnostic information. Radiological imaging mainly provides structural information, while nuclear medicine imaging adds specific functional and molecular information depending

on the chosen radiotracer. Hybrid imaging has the advantage of combining structural and functional information.

For detection and T staging of clinically significant PC, MRI has proved to be a useful imaging modality, initially for biopsy guidance in case of negative first set of systematic biopsies, but increasingly in the pre-biopsy planning stage. The superior soft tissue resolution in MRI helps localizing the tumor by distinguishing the different anatomical zones of the prostate. MRI may also be valuable in the assessment of extraprostatic extension of the tumor, although to achieve higher predictive performance, MRI findings should be assessed in combination with PSA and ISUP grade (31). For standardized MRI protocol and interpretation in PC, PIRADS version 2.1 (Prostate Imaging – Reporting and Data System) is the current state-of-the-art, as postulated by the American College of Radiologists (32). However, new findings show that multiparametric MRI (mpMRI) may be reduced to biparametric MRI with preserved ability to detect clinically significant PC (33).

A remaining challenge in PC imaging is to find a reliable method to evaluate metastases, in particular N+ disease. With standard imaging such as CT and MRI, sensitivity for LN metastases in PC is less than 40% (34). Planar BS has moderate to high sensitivity (70%) but low specificity (57%) for bone metastases in high-risk PC (35). Thus, there is a need for more accurate imaging methods to improve non-invasive N (lymph node) and M (distant metastasis) staging in PC. In the rapidly evolving field of PC imaging, the diagnostic performance of PET/CT has been demonstrated for a number of radiotracers including prostate-specific membrane antigen (PSMA), fluciclovine, choline and ACE, but their prognostic impact still remains unclear.

According to current 2019 EAU guidelines for primary staging of PC, tumor extent should be assessed by clinical examination and PSA, with supplementary information from MRI, BS and CT. PSMA-PET/CT, ^{11}C-/^{18}F-choline-PET/CT and MRI provide a more sensitive detection of LN metastases and bone metastases than BS and CT, but the effect of earlier metastasis detection on patient survival calls for further investigation (10). In the recurrent setting however, even though evidence is still weak, PET/CT can be performed if the result of imaging will influence subsequent treatment decisions. In recurrent PC, PSMA, fluciclovine and ^{11}C-/^{18}F-choline are the current radiotracers of choice (10).

Ionizing radiation and dose in medical imaging

Ionizing radiation is high-energy radiation with enough energy to detach electrons from their atoms (ionize). Two kinds of ionizing radiation contribute to the diagnostic image in medical imaging: gamma radiation from the decay of radionuclides in nuclear medicine imaging, and x-ray radiation produced outside of the nucleus by electrons in radiological x-ray and CT imaging. The harmful effects on cells exposed to ionizing radiation are either cell death or mutation of cell DNA, which may eventually lead to carcinogenesis or teratogenesis. The radiation doses associated with medical imaging therefore need to be carefully supervised. To compare the risk for late stochastic health effects (related to the probability of cancer induction and genetic effects) of radiation exposure, radiation doses for different medical imaging procedures are expressed in terms of effective dose (mSv). The effective dose concept is a generalized model weighting factors for radiation quality and organ sensitivity, and cannot be applied to individual patients.

The transformation of radionuclides into a more stable state produces ionizing radiation, either in the form of particle radiation (alpha, beta+, beta-), or electromagnetic radiation (gamma radiation), or a combination of both. This is called radioactive decay. The radiation doses from medical imaging with radionuclides depend on their proportions of alpha, beta and gamma radiation, on their gamma photon energy levels, and on the half-lives of the radionuclides. The effective half-life also takes into account the biological half-life, which is the time needed to eliminate 50% of a given substance by metabolic turnover and excretion. The effective half-life of a radionuclide for clinical use is a design consideration, balancing between the time required for diagnostic scanning, and rapid clearance to reduce excessive radiation dose to the patient and to patient surroundings.

Principle of PET/CT

PET/CT is a hybrid imaging method combining functional and molecular information from the PET, with morphological information from the CT. PET requires radionuclides that decay through positron emission. The emitted positrons from the decay encounter electrons in surrounding tissues. This encounter results in annihilation of both particles, and their mass energy is transformed into two 511 keV high-energy photons (gamma radiation), going in opposite directions. The PET scanner has a ring of closely packed scintillation detectors to localize the 511 keV photons. When two photons are detected almost simultaneously, they are assumed to originate from the same decaying radionuclide, localized somewhere along the line between the two detectors, the line-of-

response. In time-of-flight PET, the minimal time difference between the detection of the two photons is used to further improve the localization. The basic principles of PET are illustrated in figure 5.

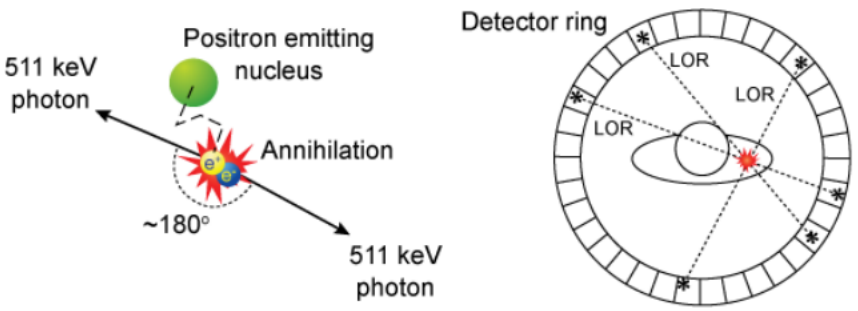

Figure 5. Basic principles of PET[2]. Image reprinted from Ganai R.et al. A Proof- of-Principle for Time of Flight-Positron Emission Tomography Imaging. In: Naimuddin M. (eds) XXII DAE High Energy Physics Symposium. Springer Proceedings in Physics, 2018; 203: 1-3, with kind permission from Springer, Cham.

All detector signals from two opposite 511 keV photons that are registered close to simultaneously are counted, and the signals from all such detector pairs form the raw data. The scintillation crystals used in PET are silicon-based: cerium-doped oxy-orthosilicates, LSO and GSO[3]. The interaction of the 511 keV photons with the scintillation crystals produces light photons, which are propagated to photo-multiplier tubes containing photo-cathodes. The light photons hit the photo-cathodes and their energy is converted into electrons, which are amplified in the photo-multiplier tubes, resulting in electrical pulses. The electrical pulses are

[2] LOR – line of response.
[3] LSO - Lu_2SiO_5:Ce. GSO - Gd_2SiO_5:Ce.

processed to produce electrical signals which carry information about the position of the captured 511 keV photons, thereby creating a 3D image of the distribution of the internal radiation.

Spatial resolution in PET is limited by factors such as positron range and size of the scintillation crystals. The registered tomographic PET raw data is reconstructed with iterative algorithms to improve resolution and minimize noise. In an iterative reconstruction (IR), an initial projected assumption of the expected activity distribution, based on tissue interaction, is made for each projection. The ratio between the projected assumptions and the actual measured projections is applied to calculate new, more appropriate, projected assumptions in the next iteration. With increasing number of iterations, the difference between the projected assumptions and the measured projections decreases, and the estimated activity distribution becomes closer to reality.

To further improve PET resolution, information about the PET detector response can be incorporated into the 3D IR algorithm.

The loss of apparent activity in small structures is called partial volume effect. In PET, partial volume effect is the result of the limited resolution.

Most of the photons from the decay are absorbed in the body, a process called attenuation. Attenuation is lower at the surface than in deep structures in the body, with the exception of the air-filled lungs which have low attenuation. In contrast, the compact skeleton has high attenuation. To reduce attenuation artifacts, the PET data is reconstructed with attenuation correction. Attenuation correction can be performed with a transmission scan with an external photon source prior to radiotracer injection, or with CT, where intensity values are correlated to tissue density. In PET/CT, attenuation correction is CT-based. The CT-

based attenuation correction is susceptible to respiratory motion artifacts and high-density materials such as metallic implants or calcifications. With the development of PET/MRI, various approaches have been developed to overcome the challenge of PET attenuation correction based on MRI, since a rotating external photon source or an integrated CT would be incompatible with the strong magnetic field (36).

In PET, volumes of interest can be defined to measure maximum and mean standardized uptake values (SUV_{max} and SUV_{mean}), functional tumor volume (FTV) and total lesion glycolysis (TLG) or the equivalent total lesion uptake (TLU). These are semi-quantitative PET parameters to aid in the evaluation of PET/CT, both in primary diagnostics and in therapy response monitoring with PET/CT over time (37,38). The SUV measurement describes the measured activity normalized to the injected activity and body weight. The definition of SUV (g/mL) is the tissue activity concentration (kBq/mL) at time T divided by the ratio of the administered dose (MBq) at time of injection, and body weight (kg):

$$SUV = Activity/(\frac{Dose}{Weight})$$

SUV_{max} is the highest pixel in a selected region-of-interest, and SUV_{mean} is the mean value of SUV of all pixels within a region-of-interest. FTV is the active volume of the region-of-interest. TLG is an established term of active disease burden, though its name refers to glycolysis (exclusive for FDG). TLU is an equivalent but more neutral term than TLG. Both TLG

and the more appropriate TLU are calculated from parameters SUV_{mean} and FTV:

$$TLU = SUVmean * FTV$$

The quality of the structural anatomical information from the CT component of hybrid imaging with PET/CT, depends on the CT imaging protocol.

CT is a tomographic method using a number of x-ray projections from different angles to create a 3D volume. The CT x-ray tube accelerates electrons from the cathode to the anode with a tube potential typically between 70 and 150 kV. When the electrons hit the anode target, some electrons will be attracted by the positive target atomic nuclei and deflect from their course, thereby losing part of their kinetic energy, which is converted into x-ray photons. This is called bremsstrahlung and constitutes the major source of radiation from an x-ray tube. X-ray radiation is a spectrum of x-ray photon energies depending on tube potential and anode angle. This is a major difference in the ionizing radiation employed in CT compared to PET, where annihilation photons have an energy of 511 keV. The CT x-ray tube potential (kV) affects the x-ray photon energy spectrum and also determines the number of photons. The energy distribution of the x-ray photons is further modified by filtration, where a portion of the low-energy photons in the x-ray photon energy spectrum is removed. Such low-energy photons would otherwise be absorbed in the patient, contributing only to patient dose and not to diagnostic information.

Image quality is determined by tube potential (kV), filtration settings and image reconstruction, but also tube current and exposure time product (mAs) influence image quality and patient dose by determining the amount of radiation. Higher tube potential increases penetration and exposure, and may improve image signal-to-noise ratio. However, higher x-ray photon energies will also increase scattered radiation and the proportion of photons without any tissue interaction, and decrease the difference in attenuation between different tissues, thereby impairing image contrast. The exposure time product (mAs) is automatically adjusted depending on the dedicated CT protocol, and may be reduced if the tube potential (kV) is increased.

The x-ray photons are transmitted through the part of the body that is examined, and are registered with photon detectors. There are several variants of modern CT systems. One common technique is the helical CT, which consists of a continuously rotating x-ray fan beam and a corresponding multi-row solid detector array. In combined PET/CT systems, the detector size is 2-4 cm, while in modern stand-alone CT systems, detectors are larger and enable axial imaging up to 16 cm in the longitudinal direction. During the rotation of the CT system, the patient table is moved with constant velocity through the gantry, resulting in a spiral data set. The field-of-view in CT is the laterolateral size of the reconstructed image and can be up to 50 cm in stand-alone CT.

After scatter reduction, the transmitted photons form the CT raw data. The CT raw data may then be reconstructed with filtered back-projection, IR algorithms, and recently deep learning algorithms, in which the detector signal is reconstructed into 3D images. CT images consist of a square matrix of elements (pixels), each of which represents a 3D volume

element (voxel) of the examined tissue. A common setting is a 512 x 512 square matrix (one for each voxel). With CT, submillimeter isotropic spatial resolution can be achieved.

The CT image is a result of the x-ray beam attenuation in a patient, where photons are either absorbed (photoelectric effect), scattered (Compton scatter) or transmitted with negligible energy loss through the patient. X-ray photons are attenuated to different extents depending on the type of tissue. To differentiate between tissues, attenuation coefficients are calculated and measured in Hounsfield units, calibrated to air = -1000, and water = 0.
The CT protocol of the PET/CT examination can be low-dose or diagnostic-dose CT. Compared to stand-alone CT, the CT part of the PET/CT has inferior image quality, due to the reconstruction of the CT data to a 70 cm field-of-view with reduced resolution to match the PET data in the PET/CT fusion images. If possible, diagnostic-dose CT should be performed with intravenously administered iodinated contrast media to improve assessment of organs and tissues.

Principle of bone scintigraphy

In nuclear medicine imaging, suitable radionuclides are combined with functional molecules, into radiotracers. Radiotracers are designed to mimic biochemical mechanisms or act as receptor ligands to depict physiological or pathological processes in the body. The radiotracers are usually administered by intravenous injection, and their decay produces gamma radiation which is detected and used to reconstruct nuclear medicine images. An optimal radionuclide for scintigraphy is ^{99m}Tc,

which has a manageable half-life of 6 h. ^{99m}Tc also decays mainly with gamma radiation, of 140 kiloelectronvolt (keV) photon energy, suitable for medical imaging.

BS is based on intravenous injection of ^{99m}Tc-labelled bisphosphonates, for instance ^{99m}Tc-hydroxymethylene diphosphonate (HDP). ^{99m}Tc is produced from the decay of ^{99}Mo in a ^{99m}Tc-generator. The ^{99m}Tc-HDP accumulates in bone and is excreted via the urine. ^{99m}Tc-HDP has greatest affinity for areas with increased osteogenesis and actively metabolizing bone (39). Increased uptake in BS reflects the biological process of increased osteoblastic activity, which is present in fracture healing, bone remodelling, osteoarthritis and osteitis, as well as in osteoblastic malignant lesions.

The attached radionuclide ^{99m}Tc decays while emitting gamma radiation. After alignment by lead collimators, the gamma radiation is captured by scintillation detectors in a gamma camera. The gamma camera scintillation detector is a light-isolated sodium iodide crystal with traces of thallium. The scintillation crystals are connected to photo-multiplier tubes, creating a 2D image in a process similar to that previously described for PET. 2D-scintigraphy may be extended to a 3D-single photon emission computed tomography (SPECT), usually combined with a low-dose CT (SPECT/CT), to improve localization of pathological uptakes. In SPECT, up to three gamma camera detectors rotate around the patient while registering gamma radiation in a number of projections. The registered tomographic SPECT data is then reconstructed, usually with IR algorithms.

Prostate cancer biomarkers in PET

In molecular imaging in PC, several PET radiotracers have been evaluated. Some of the most studied compounds are metabolic radiotracers like ACE, or compounds that bind to PSMA and gastrin-releasing peptide, or hormone receptors analogs (40–45).
An overview of potential molecular targets is illustrated in figure 6.

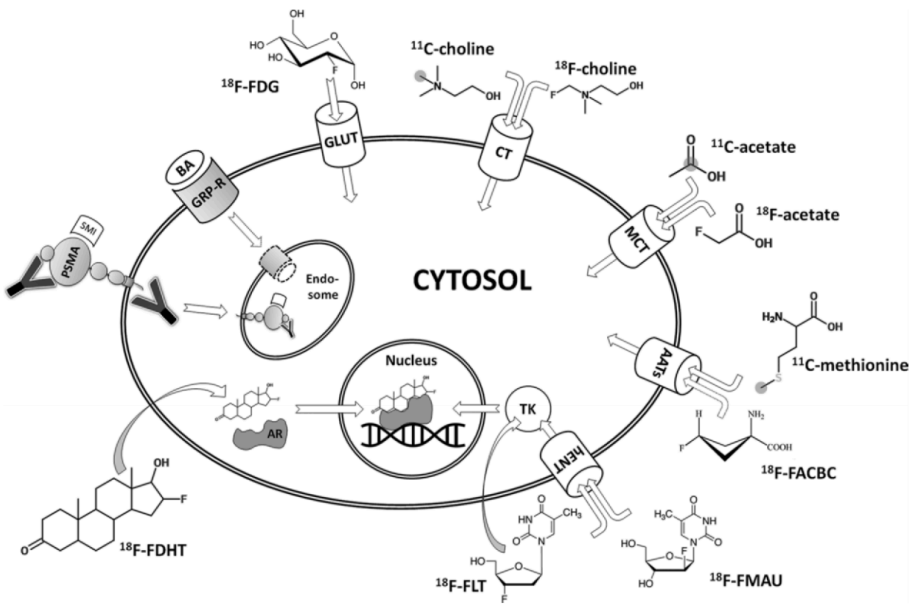

Figure 6. Overview of potential PET/CT targets in prostate cancer[4]*. Image reprinted from Wibmer et al. Molecular imaging of Prostate Cancer. RadioGraphics 2016; 36: 142-161, with kind permission from the Radiological Society of North America.*

[4] FACBC - anti-1-amino-3-^{18}F -fluorocyclobutane-1- carboxylic acid. DCFBC - (N-[N-[(S)-1,3-dicarboxypropyl]carbamoyl]-4-F-fluorobenzyl-L-cysteine). DCFPyl - 2-(3-{1-carboxy-5-[(6-^{18}F-fluoro-pyridine-3-carbonyl)-amino]-pentyl}-ureido)-pentanedioic acid.
GRP - gastrin-releasing peptide. FHDT - ^{18}F-fluorodihydrotestosterone. AATs - amino acid transporters. AR - androgen receptor. BA - bombesin analog- CT - choline transporter. GLUT - glucose transporter. GRP-R - gastrin-releasing peptide receptor. hENT - human equilibrative nucleoside transporter. MCT - monocarboxylate transporter. SMI - small molecule inhibitor. TK - thymidine kinase. Y - antibody.

Although choline radiotracers have been used more extensively, comparative studies between ^{11}C-/^{18}F-choline and ACE, have shown equal diagnostic performance and accuracy in recurrent PC (41,46,47). Buchegger et al. showed for instance excellent agreement between ^{18}F-choline and ACE in the detection and localization of positive LNs and skeletal metastases in PC (46). ^{11}C-choline-PET/CT has proved valuable mainly for radiotherapy planning in biochemical recurrence after radical prostatectomy (48). Data is promising regarding the more recent PSMA radiotracers. In a review article addressing the different PET radiotracers considered for guidance prior to extended pelvic LN dissection in PC, ^{18}F/^{11}C-choline and PSMA radiotracers were found to be the most valuable (49). A recent review on theranostics in PC has shown that ^{68}Ga-PSMA-PET/CT is superior to ^{18}F/^{11}C-choline-PET/CT in both primary staging and restaging (50).
In a recent article on PET in primary staging and risk assessment of PC, the authors conclude that further studies of existing radiotracers and the development of novel future radiotracers can be expected, as the optimal radiotracer for PC has not yet been identified (44).

^{11}C-acetate

Acetate is an intermediary energy substrate involved in fatty acid metabolism, as the main carbon source for cytosolic lipid synthesis. Acetate is converted by acetyl-CoA synthetase to acetyl-CoA. There are two kinds of acetyl-CoA synthetase, mitochondrial and cytosolic, of which the mitochondrial variant is upregulated in many cancer types, such as PC, hepatocellular carcinoma, glioblastoma and breast cancer

(51,52). To meet the increased energy demands of cancer cells, the acetyl-CoA produced in the mitochondria acts as an energy substrate within the Krebs cycle, and is metabolized to CO_2. The acetyl-CoA that is produced in the cytosol is in turn converted by fatty acid synthase into fatty acids. Fatty acid synthase catalyzes fatty acid biosynthesis in the cell membrane and is overexpressed in PC (28). Increased acetate uptake due to increased fatty acid synthase activity in cells has been shown to correlate with aggressiveness of PC (53).

The radiotracer ACE thus reflects increased lipid metabolism and cell membrane synthesis in PC cells, making primary tumors and metastases detectable by ACE-PET/CT (41).

The physiological ACE uptake is high in the pancreas, spleen, liver and salivary glands, while the uptake is variable in the heart, muscles and skeleton (54). Liver uptake of ACE has been shown to increase in patients with hepatic steatosis (55). ACE is mainly excreted as CO_2 by the respiratory system, and is only occasionally seen in the urinary system, which is advantageous in the evaluation of structures adjacent to the urinary bladder, such as the prostate and pelvic LNs.

A limitation to be aware of, with ACE being a metabolic radiotracer, is that increased uptakes, especially in LNs as part of the immune system, can occur for reasons other than PC-induced metabolic changes. Such factors include inflammatory, reactive and degenerative conditions, causing false positive findings (56). This limitation can be diminished with the use of a diagnostic CT as part of the PET/CT, to facilitate and improve the interpretation of the findings. One should bear in mind, however, that the issue of LN assessment is a general challenge in medical imaging.

In addition, increased ACE uptake may be seen in other slow-growing tumors than PC. Some of the recognized and studied ACE-avid tumors except for PC are highly differentiated hepatocellular carcinoma, renal cell carcinoma, indolent lymphoma, bladder carcinoma, brain tumors including meningioma and adenoma of the pituitary gland, gastric adenocarcinoma and multiple myeloma (56–61). In cerebral glioma, ACE-PET/CT has been found to predict tumor differentiation and survival (62).

In non-oncological applications, ACE has been most studied as a non-invasive marker of myocardial oxidative metabolism and myocardial blood flow on a segmental level, through estimation of clearance rates of ACE assessed by dynamic PET (63,64). ACE uptake has also been described in Paget's disease of the bone. (65).

A methodological limitation with ACE is the short half-life of ^{11}C ($T_{1/2} \approx$ 20 minutes), which requires on-site cyclotron and radiochemistry facilities. The use of the more long-lived radionuclide ^{18}F ($T_{1/2} \approx 110$ minutes) rather than ^{11}C would facilitate the administration, but unfortunately, 2-[^{18}F]- fluoroacetate is not a functional analog of 1-[^{11}C]-acetate and is not suitable for studies of lipid synthesis, intermediary metabolism or myocardial oxidative metabolism (66).

^{11}C-acetate-PET/CT in prostate cancer

The main clinical applications for ACE-PET/CT appear to be primary staging and restaging of intermediate- and high-risk PC prior to radiotherapy (40,67–71). A meta-analysis with 24 studies showed a sensitivity and specificity of ACE-PET/CT in primary DIL detection of 75% and 76%, and in local recurrence 64% and 93%, respectively (70).

In a more recent study of ACE-PET/CT in biochemical relapse, an impressive detection rate of 88% for the site of recurrence/metastasis was demonstrated (72). In the same study, the authors suggested that a PSA threshold of >1.09 ng/mL or a PSA doubling time of < 3.8 months when the PSA is below 1.0 ng/mL, could represent independent predictors of ACE positivity in biochemical relapse (72).

For N staging, sensitivity and specificity numbers of ACE-PET/CT are more divergent, ranging from 38-68% and 78-96% in different studies of intermediate- and high-risk PC with histopathological confirmation (69,73,74). Schumacher et al. concluded that the limited ability to detect microscopic LN involvement on lesion basis makes extended pelvic LN dissection essential in all patients diagnosed with positive LNs on ACE-PET/CT (74). On patient basis, Esch et al. showed a positive predictive value for detection of LN metastases in ACE-PET/CT of 76%, as verified by histopathology or decline in PSA after radiotherapy, in a study of PC patients with biochemical relapse (75).

A systematic review and meta-analysis comparing ^{11}C-/^{18}F-choline-PET/CT and mpMRI in detection of LN metastases in PC, found that ^{11}C-/^{18}F-choline-PET/CT performed better on both patient basis and nodal basis, although sensitivity was suboptimal on nodal basis (76). A study on ACE-PET/mpMRI from 2017 showed a sensitivity, specificity, and diagnostic accuracy for the detection of LN metastases of 100%, 96%, and 97% on region basis, with histopathology as reference standard (77). Hybrid ACE-PET/mpMRI improved diagnostic accuracy of LN metastases on region basis, compared to stand-alone mpMRI (77). In summary, studies indicate that LN detection with ACE-PET/CT is

suboptimal on nodal basis, while it seems to be of value on patient basis and possibly on region basis.

It has been suggested that one of the main applications for ACE-PET/CT in PC is to rule out distant metastases prior to salvage radiotherapy in early biochemical relapse (40). As regards detection of distant metastases, a meta-analysis of ^{11}C-choline-PET/CT showed higher specificity for bone metastases compared to planar BS (78). It seems reasonable to assume that this holds true also for ACE but more evidence is needed, since ACE reflects a different biochemical mechanism than ^{11}C-choline, although they resemble each other in terms of cell membrane synthesis. In a pilot study of ACE-PET/CT and FDG-PET/CT in eight BS-positive PC patients, ACE-PET/CT showed promising results (79), and in the above mentioned study on ACE-PET/mpMRI, four patients were correctly found to have bone metastases, and one a liver metastasis, all confirmed by histopathology (77). Otherwise, data on the diagnostic accuracy of ACE-PET/CT in distant metastases is limited.

Long-term survival data on PC relapse patients examined with ^{11}C-choline-PET/CT showed a 15-year PC-specific survival probability of 42% in PET-positive patients and 96% in PET-negative patients (80). No such prognostic long-term data is yet available for ACE-PET/CT. However, a study of ACE-PET uptake as a biomarker for malignant lipogenesis and its impact on survival in patients with biochemical relapse after radical prostatectomy, showed an 80% 5-year PC-specific survival in patients with a positive PET/CT, in contrast to 100% in patients with negative PET/CT (38). Highest lesion SUV_{max} and total lipogenic activity correlated with time-to-death, suggesting that lipogenic

ACE-PET/CT parameters might provide useful prognostic information (38). The prognostic potential of ACE-PET/CT has also been proposed in primary staging by Haseebuddin et al. (69), who showed that ACE-PET positivity at baseline prior to radical prostatectomy predicted treatment failure in intermediate- and high-risk PC. Treatment-failure-free survival was poorer in PET-positive than in PET-negative patients, interestingly also in those considered as false-positive with regards to histopathology (69). In a recent study of ^{11}C-choline-PET/MRI in primary staging of high-risk PC, metabolic tumor volume and uptake volume product were significantly associated with shorter progression-free survival, further supporting the added value of baseline PET volumetric parameters as prognostic biomarkers (81).

In a cohort of patients with metastatic castration-resistant PC, treatment response evaluation at follow-up ACE-PET/CT significantly predicted outcome, where patients with progressive disease on PET/CT had significantly shorter progression-free survival and overall survival than those with partial response or stable disease (82). In the same study, PSA response to treatment (>50% reduction) was also found to predict progression-free survival and overall survival. Authors suggested that treatment response evaluation with ACE-PET/CT therefore may be of particular prognostic added value in metastatic castration-resistant PC, in the subgroup lacking a PSA response due to tumor dedifferentiation (82).

In summary, ACE-PET/CT seems to be of value for primary staging and restaging of intermediate- and high-risk PC, in particular to rule out distant metastases. ACE-PET/CT has shown varying performance in LN assessment, high-lighting a general problem in medical imaging with

differentiating malignant from reactive LNs. The prognostic value of ACE-PET/CT has been indicated in both primary and relapse settings, but there is still a need for studies with more long-term data.

Specific background of the studies

The PARAPLY study

The PARAPLY study, "PAtients receiving RAdiotherapy for Prostate cancer with high risk for LYmph node metastasis" (Phase 2 Study of High Risk Prostate Cancer Treated With Dose-escalated Simultaneous Integrated Boost to the Prostate and Lymph Node Gross Tumor Volumes) is a prospective single-arm interventional phase 2 study. The main aim is to assess the outcome of imaging-guided dose-escalation with simultaneous integrated boost to the suspected DIL and pelvic LN metastases, in patients with high-risk PC. The boost volumes are outlined with ACE-PET/CT and mpMRI. The concept of external-beam radiotherapy planning guided by PET/CT in PC has been investigated in multiple studies, but the effect on progression-free survival and overall survival is still unknown (83). The hypothesis is that the intervention group will have less relapses compared to matched historical controls, due to improved delineation of gross tumor volume. Patients without a distinct DIL or suspected LN spread receive the current standard radiotherapy field, covering the prostate and the seminal vesicles (78 Gy). The primary outcome measure is progression-free survival (time-frame 36 months).

Patients in paper I and II of this thesis were part of the start-up for the PARAPLY study, and patients in paper IV were prospective PARAPLY study participants.

Paper I

High-risk PC patients may be cured with radiotherapy or radical prostatectomy. Reliable treatment planning tools are crucial to enable personalized treatment, such as adding simultaneous integrated boost against the suspected DIL and pelvic LN metastases to the standard radiotherapy field. The lack of an accurate imaging method for LN assessment has to this date resulted in the routine use of clinical nomograms for estimation of the risk of pelvic LN metastases. ACE-PET/CT may provide an added diagnostic value compared to the standard method clinical nomogram, in personalized LN assessment.
In a study on recurrent PC, prostate tumor SUV_{max} ($SUV_{max,DIL}$) correlated with initial GS, and patients with a high PSA velocity proved to have higher lesion SUV_{max} on ACE-PET/CT (84). Authors concluded that $SUV_{max,DIL}$ could serve as a prognostic marker in recurrent PC (84). In a recent study on the value of mpMRI and ACE-PET/CT in primary staging of intermediate- and high-risk PC, LN SUV_{max} ($SUV_{max,LN}$), but not $SUV_{max,DIL}$, was a predictor of regional LN metastasis but did not outperform mpMRI (85). It has been shown that there is an overlap in SUV_{max} between PC and benign prostatic hyperplasia in ACE-PET/CT, thereby impairing the $SUV_{max,DIL}$ assessment (86). Thus the research question remains whether the level of $SUV_{max,DIL}$ might be associated with and serve as a predictor of N+ disease on PET/CT. The main aim of this study was to assess the added diagnostic value of ACE-PET/CT to

clinical nomogram in primary staging of high-risk PC, by evaluating the association between LN detection rate on ACE-PET/CT and clinical nomogram risk. The second aim was to evaluate the association between $SUV_{max,DIL}$ and N+ disease on PET/CT.

Paper II

BS is a standard method in clinical routine for detection of bone metastases in high-risk PC (87). Despite the development of medical imaging in PC, BS is still among the recommended first-hand methods for primary staging in the 2019 EAU guidelines. A well-known limitation with BS for cancer staging purposes, is that increased uptake merely reflects the unspecific biological process of increased osteoblastic activity. ACE-PET/CT may provide an added diagnostic value compared to the standard method BS. While actual data on ACE-PET/CT in bone metastases is sparse but promising (79), data on ^{11}C-choline further indicates the diagnostic value of ACE in bone metastases (46,78).
The aim of this study was to assess the added diagnostic value of ACE-PET/CT to BS in primary staging of high-risk PC, by comparison of detection rates of bone metastases with ACE-PET/CT and BS, and by validation of the results with follow-up data.

Paper III

PET data is reconstructed with different IR algorithms. For ACE-PET/CT, VUEPointHD™ ViP (VPHD) (GE Healthcare, WI, US) and VUEPointHD™ SharpIR (SharpIR) (GE Healthcare, WI, US) algorithms may be used. SharpIR improves PET resolution by incorporating PET

detector response information into the 3D IR algorithm, so-called resolution recovery. The spatial resolution for VPHD is 6 mm (FWHM[5]), and for SharpIR 3 mm. The resolution recovery algorithm should produce more accurate PET measurements in terms of $SUV_{max,}$ SUV_{mean}, FTV and TLG, than the Ordered Subsets Expectation Maximization (OSEM)-based VPHD, without resolution recovery. Compared to VPHD, SharpIR should produce smaller FTV and TLG because of the improved resolution, and higher SUV_{max} and SUV_{mean} because of the reduction of partial volume effect.

The region-of-interest delineation algorithm (SUV threshold) may have a significant impact on FTV, making the SUV thresholding algorithm a relevant methodological factor in radiotherapy planning. The 42% threshold has been shown to produce reliable FTVs in numerous publications (88–91). In order to further improve SUV thresholding, an adaptive estimated thresholding algorithm for region-of-interest delineation has been developed and supplied with the PET-VCAR software in the GE Advantage Workstation (GE Healthcare, WI, US).

Decreasing PET acquisition time may be feasible if sufficient image quality and quantitation are preserved. Shorter acquisition time would facilitate for patients to undergo ACE-PET/CT, and likely reduce patient movement artefacts. Because of the short half-life of ^{11}C ($T_{1/2} \approx 20$ minutes), a whole-body scan will reflect different amounts of radioactivity at different bed positions. Shorter PET acquisition time may increase image quality by maintaining a more comparable amount of radioactivity during the examination, regardless of bed position.

[5] FWHM – full width at half maximum, an expression of spatial resolution in imaging.

The aims of this study were to optimize PET reconstruction algorithm, SUV thresholding algorithm and PET acquisition time for ACE-PET/CT.

Paper IV

The prognostic potential and added value of ACE-PET/CT in PC have been addressed in previous publications (38,69). However, additional preferably prospective clinical studies are necessary to confirm the associations between lipogenic PET biomarkers and prognostic outcomes time-to-progression and progression-free survival. The long-term perspective needed for such assessment calls for interim analyses.
An approach to indirectly assess the added prognostic value of ACE-PET/CT, is to evaluate the associations between lipogenic PET biomarkers and known clinical risk parameters.
In paper III, PET reconstruction with resolution recovery, SharpIR (GE Healthcare, WI, US), was shown to improve quantitative measurements of ACE-PET parameters as compared to phantom studies and structural CT information (92). However, the clinical significance of adding SharpIR has not yet been shown. Thus, further studies of the possible prognostic potential of lipogenic ACE-PET/CT biomarkers, using both PET reconstruction algorithms, are motivated.
The aim of this study was to indicate the possible added value of ACE-PET/CT in pre-therapeutic risk assessment, by analyzing associations between clinical risk parameters and baseline ACE-PET/CT-derived parameters, in primary staging of high-risk PC.

Aims

The aims of this thesis were to:

I

- evaluate the added diagnostic value of lipogenic ACE-PET/CT biomarkers in primary staging of high-risk PC, with focus on N staging.

II

- evaluate the added diagnostic value of lipogenic ACE-PET/CT biomarkers in primary staging of high-risk PC, with focus on M staging.

III

- identify and validate optimal PET reconstruction algorithm and SUV thresholding algorithm in ACE-PET/CT.

IV

- indicate the possible prognostic value of lipogenic ACE-PET/CT biomarkers in pre-therapeutic risk assessment of high-risk PC.

Materials and Methods

Patients

Paper I and II

The patients in paper I and II were from the same cohort: patients referred to the Nuclear Medicine section, Department of Radiology, University Hospital of Umeå, for primary staging with ACE-PET/CT of biopsy-verified high-risk PC, prior to radiotherapy with curative intention.

For paper I, the 49 first consecutive patients from the described cohort examined between 2011 and 2013, with known nomogram risk, were included.

For paper II, the first 66 consecutive patients from the described cohort examined between 2011 and 2014, with a comparable BS within 3 months, were included.

Both study I and II were approved by the Regional Ethics Review Board (approval number 2013-154-31) as part of the start-up for the larger PARAPLY study. All participants had previously accepted to take part in the clinical routine work-up.

Paper III

Sixteen consecutive ACE-PET/CT scans performed in the setting of primary staging or restaging, between September 2014 and November 2014 were included in paper III. Inclusion criteria were biopsy-verified high-risk PC with >15% nomogram risk of pelvic LN metastases, and pathological ACE uptake in the prostate and/or in pelvic LNs.

To simulate a variety of lesions, a phantom with <0.1 mm wall thickness was constructed, with seven spherical interventional balloons of different sizes. All balloons were filled with the same concentration of FDG, in 0.1- 9.2 cm^3 volumes. The FDG in the balloons was allowed to decay throughout the experiment, with activity concentrations decreasing from 73.5 to 32.4 kBq/mL. New FDG was continuously added to the background, to achieve PET scans with different signal-to-background (S/B) ratios, in the range of 15.9 to 4.3.

Paper IV

All eligible participants from the PARAPLY study with a contrast-enhanced CT as part of the baseline ACE-PET/CT, a total of 67 patients, were included. All patients were diagnosed with high-risk PC and underwent ACE-PET/CT for primary staging between 2013 and 2017. Exclusion criteria were disseminated disease or other malignancies that might interfere with disease assessment or life expectancy.

Ethical considerations

Study I-IV were approved by the Regional Ethics Review Board and the Radiation Safety Committee of Umeå University Hospital.
In all medical imaging involving ionizing radiation, radiation doses should be kept as low as reasonably acceptable for diagnostic purposes, to reduce the risk of radiation-induced carcinogenesis, and if applicable, teratogenesis. Medical imaging procedures must be justified in terms of risk versus benefit. The imaging methods used in this thesis, ACE-PET/CT and BS, were performed on men with high-risk PC. Effective

patient dose from ACE was approximately 1 mSv. Few dosimetry studies are published on ACE, but in a dual tracer study on ACE- and FDG-PET/CT for staging of hepatocellular carcinoma, patient-specific effective dose from ACE was 1.56±0.47 mSv (93), endorsing the dosimetric reproducibility.

Effective patient dose from CT was approximately 15 mSv. Effective patient dose from ^{99m}Tc-HDP was approximately 2,5 mSv. For the patient cohort described in this thesis, the radiation doses pertaining to the imaging methods were small, compared to the therapeutic radiation doses from the radiotherapy.

Changing therapy approach based on findings in an imaging method still under investigation may not be considered as evidence-based practice. However, patients with high-risk PC have poor prognosis, and the risk of negative side effects from added radiotherapy boost is low. In this setting, the possible benefit should outweigh the potential harm. In the reverse perspective, before patients were excluded from curative treatment, there had to be convincing evidence of distant metastases, not only based on ACE-PET, but on other established imaging methods, clinical consensus, and if necessary, histopathological confirmation.

Imaging

The PET/CT examinations were performed with a GE Discovery 690 PET/CT scanner (GE Healthcare, WI, US). PET scanning was commenced 10 minutes after intravenous injection of 1-[^{11}C]-acetate (4.0 MBq/kg body weight), in time-of-flight mode. PET acquisition time was 2 minutes/bed position, from the proximal femur to the head. PET data was reconstructed with the OSEM-based 3D IR algorithm

VuePointHD™ (GE Healthcare, WI, US), corrected for attenuation and scatter.

In paper III and IV, PET data was also reconstructed with a second IR algorithm, SharpIR, with added resolution recovery in the IR loop.

Standard examinations included a diagnostic contrast-enhanced CT (Omnipaque 350 mg iodine/mL, 0.5 g iodine/kg), with 50 cm field-of-view. In patients with impaired renal function, recent contrast-enhanced CT within the last month, or previous contrast reaction, the diagnostic CT was performed without contrast media.

The BS examinations in paper II were acquired with an Infinia Hawkeye 4 gamma camera (GE Healthcare, WI, US), with whole-body anteroposterior and posteroanterior scans 2.5 h post-injection of 550 MBq ^{99m}Tc-HDP, according to European Association of Nuclear Medicine guidelines (94).

PET parameters

SUV_{max} (g/mL), SUV_{mean} (g/mL), FTV (cm^3) and TLG or TLU ($g \cdot cm^3/mL$) were measured for each lesion, using the PET-VCAR software in the GE Advantage Workstation (GE Healthcare, WI, US). Regions-of-interest were defined by visually selecting search areas with increased non-physiological uptakes, including a margin extending outside the uptake, with subsequent automatic region-of-interest delineation with a fixed 42% threshold relative SUV_{max}. In paper III, the above mentioned PET parameters were measured also with the estimated thresholding algorithm supplied with the PET-VCAR software, after visual confirmation that only the intended structures were included.

The phantom measurements of SUV_{max}, SUV_{mean} and FTV, were compared with the true values from the known activities in the phantom, as expressed by recovery coefficients (RC) for each parameter:

$$RC = (measured\ value)/(true\ value)$$

In paper IV, in addition to the PET parameters mentioned above, SUV_{max}, FTV, and TLU were reported in global, DIL and LN measures. Global TLU was calculated as the sum of all lesion TLUs in each patient. Global FTV was likewise calculated as the sum of all lesion FTVs in each patient.

Image analysis

In paper I-III, two physicians, double licensed in radiology and nuclear medicine, read and reported all PET/CT examinations with access to referral data and previous imaging, according to clinical routine. Any case of inter-observer disagreement was solved with consensus.
In paper IV, all included clinical PET/CT examinations were re-read at minimum 2 years after the examination date in a blinded manner by one physician licensed in radiology and nuclear medicine.
To visually assess a pathological uptake and discriminate it from the physiological background may be a delicate matter, where the reader's experience of the particular radiotracer plays a vital role. In order to standardize readings, a background reference is necessary. Traditionally, the mediastinal or liver background have been used as reference in other radiotracers. The ACE uptake in the mediastinum is lower than that of FDG, which makes mediastinal background less useful as reference. The

liver uptake, as with FDG, is irregular and high. The same goes for the spleen, although a method with a tumor-to-spleen ratio has been described to standardize the evaluation of SUV_{max} in ACE-PET (84).
In lack of a better alternative, the traditional mediastinal background was used as reference in the studies included in this thesis, but the level of ACE uptake constituted only a part of the total imaging information contributing to the final assessment of each lesion. The grade of suspicion of LN metastasis was based on the combination of SUV_{max} and any of the following generally accepted criteria for morphological changes in LNs: rounded shape, short-axis diameter exceeding 10 mm, lack of fat-containing hilus, irregular/diffuse border and visually increased contrast enhancement. Another vital aspect in the interpretation of LNs is the anatomical region and its likelihood of being affected by lymphatic spread from PC. The previously described sentinel node regions are the first regions along the lymphatic drainage route for PC. Therefore LNs in these pelvic and distant paraaortal regions should be extra carefully assessed. On the other hand, LNs with low to moderate ACE uptake and normal morphological appearance along cervical vessels and in the axillary, hilar, mediastinal and inguinal regions, where lymphatic metastases from PC are less likely to occur, are common and considered unspecific. These LNs were not reported unless they showed morphological signs on CT raising the suspicion of metastasis.
Suspected bone metastases from PC were characterized as focal uptakes visually exceeding skeletal background, with or without sclerotic and/or lytic lesions. BS was evaluated visually, as in clinical routine. BS uptakes that could be related to a history of previous trauma or degenerative

changes were considered non-metastatic. Any other increased non-physiological BS uptakes were considered metastatic.

Clinical consensus and follow-up evaluation

In paper II, pre-treatment consensus decision was made by the oncologist in discordant cases, where patients were diagnosed at baseline with bone metastases or not, after interpretation of biochemical parameters (PSA, blood count and alkaline phosphatase), clinical symptoms (localized skeletal pain) and existing baseline imaging findings (ACE-PET/CT, BS, MRI or other modality). Since ACE-PET/CT influenced pre-treatment consensus decision, the ACE-PET/CT results were not compared with pre-treatment consensus to avoid circle evidence. Instead, clinical follow-up consensus (clinical evaluation, all available imaging, biochemical parameters as above) was collected from medical records in the discordant cases, for comparison with ACE-PET/CT and BS results.

Statistical analysis

All statistical analyses were performed in IBM® SPSS Statistics 21-24 (IBM Corporation, Armonk, NY, USA). The chosen significance level was $p < 0.05$.

Paper I

Different risk groups from estimated nomogram risk of pelvic LN metastases, were compared with regards to their actual observed frequency of N+ disease with Pearson's chi-square test. Initially, nomogram risk was divided into three groups, and in a second analysis

into two groups. The associations between possible predictors $SUV_{max,DIL}$, PSA and GS, and the outcome N+ disease, were evaluated with binary logistic regression analysis. Associations between $SUV_{max,DIL}$, PSA and GS were evaluated using linear regression analysis.

Paper II

Detection rates of suspected bone metastases with ACE-PET/CT and BS were compared on patient basis with the Fischer exact test. Cohen's kappa coefficient was used to calculate the degree of agreement between ACE-PET/CT and BS, and to compare the performance of both methods with clinical follow-up.

Paper III

Measurements with SharpIR and VPHD reconstructions of SUV_{max}, SUV_{mean}, FTV and TLG, were compared with paired t-tests. Paired t-tests were also used to evaluate differences between the two thresholding algorithms, and between different acquisition times in clinical ACE-PET/CT.

DILs and suspected LN metastases were evaluated in global measurements and in separate subgroups. Also in the subgroup analyses, measurements with SharpIR and VPHD reconstructions of the above mentioned PET parameters, were evaluated with paired t-tests. In addition, observed differences in the subgroup data were evaluated with related-samples Wilcoxon signed rank test because of the small subgroup sample size.

Correlation between FTV and STV was calculated with Pearson’s correlation coefficient.

Paper IV

Differences in clinical risk parameters and ACE-PET/CT-derived parameters in relation to N+ were evaluated with binary logistic regression analysis. Due to the small sample size, all parameters could not be simultaneously evaluated in the same regression model. Therefore, logistic regression analysis was performed with focus on the most relevant parameters $SUV_{max,DIL}$, TLU_{DIL} (SharpIR reconstruction) and nomogram risk.

Correlations between nomogram risk and ACE-PET/CT parameters $SUV_{max,DIL}$, TLU_{DIL}, $SUV_{max,LN}$, TLU_{LN} and global TLU (SharpIR reconstruction) were evaluated with linear regression analysis. The linear regression models with the highest adjusted R^2 were selected.

Correlations between DIL and LN PET parameters were evaluated in linear regression analyses of $SUV_{max,DIL}$, TLU_{DIL}, $SUV_{max,LN}$, and TLU_{LN} (SharpIR reconstruction). Also correlations between the clinical parameters were evaluated with linear regression.

Correlations between ACE-PET/CT parameters global TLU and global FVT measured with VPHD and SharpIR, were evaluated with Spearman's correlation coefficient for continuous non-linear and non-normally distributed parameters.

Results

Paper I

Patients were divided into three groups according to estimated nomogram risk of pelvic LN metastases: <15% (n = 12), 15-45% (n =24) and >45% (n = 13). The observed proportions of N+ disease were 33, 33 and 69%, respectively, in the three groups. Figure 7 illustrates an ACE-avid suspected pelvic LN metastasis, with short-axis diameter less than 10 mm.

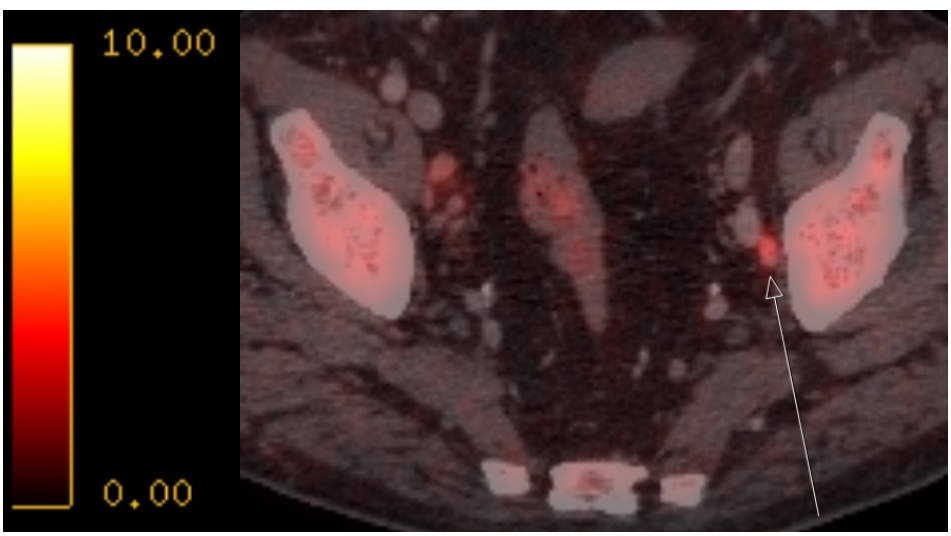

Figure 7. Transaxial PET/CT fusion showing an ACE-avid left-sided small pelvic LN, suspected for LN metastasis (arrow). The PET color scale to the left is valid also for PET/CT fusions in figures 8 and 10.

The Pearson chi-square test displayed no significant association between the observed proportion of N+ disease and the nomogram risk of pelvic LN metastases in the three original groups (p = 0.08). When dividing the

patients into only two risk groups, those with ≤45% nomogram risk had N+ disease in 33% (12/36), and those with >45% risk had N+ disease in 69% (9/13), and this association proved to be significant ($p < 0.05$).
The mean nomogram risk of pelvic LN metastases was 32%, while the mean observed proportion of N+ disease was 43% (21/49).

Binary logistic regression analysis proved $SUV_{max,DIL}$ to be higher in patients with N+ disease, with odds ratio 1.45 ($p < 0.05$). N+ disease was not associated with PSA, nor with GS. There was no significant association between $SUV_{max,DIL}$, PSA or GS and the presence of suspected distant metastases.
$SUV_{max,DIL}$ showed a significant positive correlation with PSA (Pearson correlation coefficient 0.35, $p < 0.05$), but not with GS. PSA and GS showed negative correlation -0.33, $p < 0.05$).
ACE-PET/CT influenced treatment in 43% (20/47) of the patients (data missing in two patients).

Paper II

ACE-PET/CT proved significantly superior to planar BS in detecting suspected bone metastases on patient basis in high-risk PC (Fischer exact test, $p < 0.01$). Figure 8 illustrates a discordant example of ACE-PET/CT and BS from the same patient.

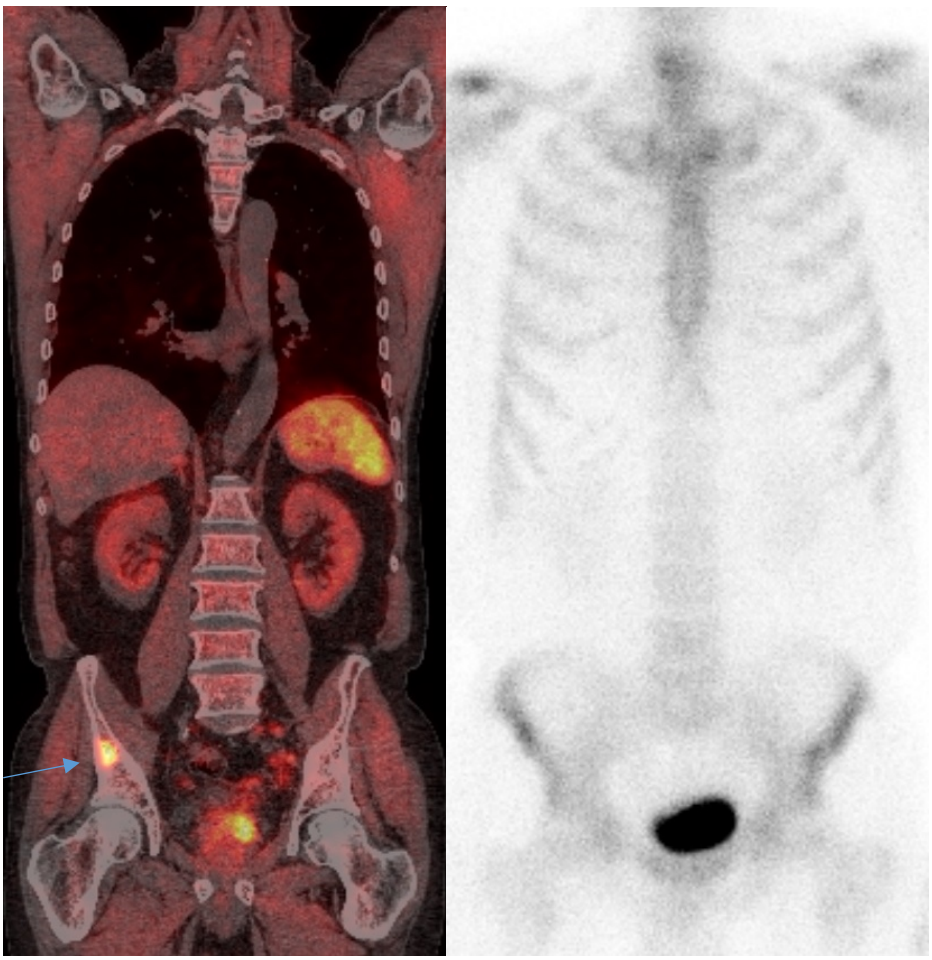

Figure 8. Coronal ACE-PET/CT fusion and anteroposterior BS from the same patient, within comparable time-frame (3 months). ACE-PET/CT reveals a focal intense uptake in the right iliac bone. Even in retrospect, the BS is not convincing for metastasis. The PET color scale is illustrated in figure 7.

ACE-PET/CT and BS did however show corresponding results in 88% (58/66) of the patients.

Kappa values were 0.64 for ACE-PET/CT compared to BS, 0.95 for ACE-PET/CT compared to clinical follow-up consensus, and 0.66 for BS

compared to clinical follow-up consensus. ACE-PET/CT influenced treatment in 11% (7/66) of the patients.

Paper III

SharpIR provided significantly higher lesion SUV_{max} and SUV_{mean}, and lower FTV and TLG, compared to VPHD.

Average SUV_{max} was 1.67 times higher with SharpIR than with VPHD ($p < 0.0001$), with both thresholding algorithms, and average SUV_{mean} was up to 1.35 times higher with SharpIR than with VPHD with 42% threshold ($p < 0.0001$).

The smallest average FTV and TLG were obtained with SharpIR 42%, while the largest average FTV and TLG were acquired with VPDH with estimated threshold.

Figure 9 illustrates two ACE-avid pelvic LNs with VPHD and SharpIR for visual comparison.

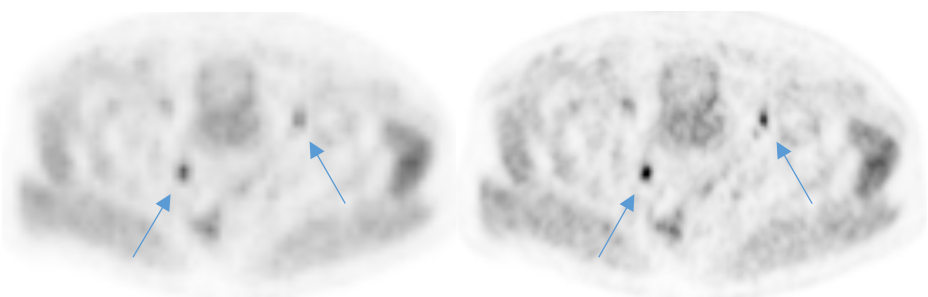

Figure 9. Increased ACE uptake in small bilateral parailiac suspected LN metastases (arrows). ACE-PET with VPHD (left) and SharpIR (right) PET reconstruction algorithms, with identical level color scale.

SUV_{max} was unaffected by thresholding algorithms. SharpIR and VPHD measurements of SUV_{mean}, FTV and TLG differed more with 42% threshold than with estimated threshold.
SUV_{max} and SUV_{mean} were overall unaffected by different acquisition times. FTV was significantly higher with longer acquisition times with both thresholding algorithms. Average FTV differed more from 1 to 2 minutes, than from 2 to 4 minutes acquisition time per bed position. Signal-to-noise ratio was clearly impaired with 1 minute acquisition time, compared to 2 and 4 minutes, which both rendered acceptable image quality.

Paper IV

In patients with N+ disease, $SUV_{max,DIL}$ and TLU_{DIL} were significantly higher than in patients with N- disease, with odds ratio 1.29 (p 0.045) and 1.04 (p 0.005), respectively. Thus, patients with N+ disease had higher lipogenic tumor burden in the prostate. There was no significant association between N+ and nomogram risk.
Significant positive correlation was found between nomogram risk and TLU_{DIL}, with an increase in nomogram risk of 0.004 per TLU_{DIL} unit (p <0.01). Thus, the higher the TLU_{DIL}, the higher the nomogram risk. Significant positive correlations were also found between TLU_{DIL} and TLU_{LN}, with an increase in TLU_{DIL} of 1.31 per TLU_{LN} unit (p 0.001), and between nomogram risk and other clinical parameters PSA, GS and T stage (p <0.001).

An example of a patient with N+ disease and high lipogenic tumor burden in the prostate is illustrated in figure 10.

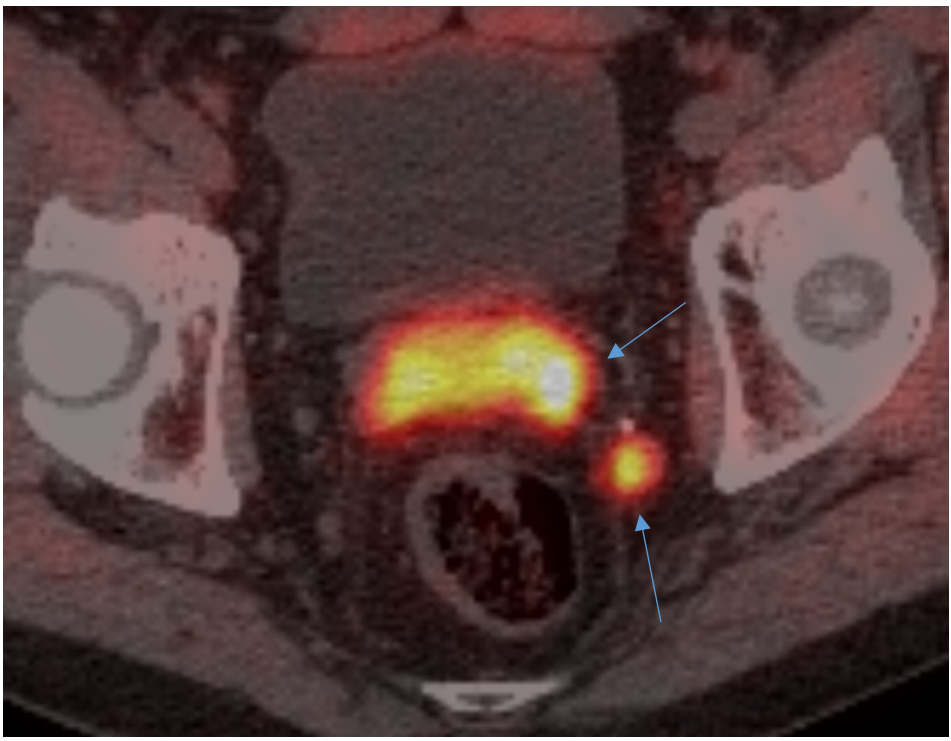

Figure 10. Transaxial ACE-PET/CT fusion in a patient with high TLU_{DIL} and N+ disease. The increased ACE uptake involves most part of the enlarged prostate, with an intense focus in the left dorsal peripheral zone (upper arrow). There is also intense ACE uptake in an enlarged left-sided metastatic pelvic LN (lower arrow). The PET color scale is illustrated in figure 7.

SharpIR was superior to VPHD and stand-alone contrast-enhanced CT in detection of N+ disease, on lesion basis as well as on patient basis. There was a statistically significant correlation between measurements with

VPHD and SharpIR, of global TLU and global FTV ($p < 0.005$, Spearman's correlation coefficients 0.88 and 0.90, respectively).

Discussion

The rationale for this thesis is the possibility of curative therapy for high-risk PC patients, where proper pre-therapeutic staging is essential for a successful outcome. Recent advances in medical imaging, particularly the identification of several suitable PET radiotracers, have improved staging of high-risk PC, but the prognostic value of this information is still unknown. The main ambition with this research has been to assess the possible added diagnostic and prognostic value of lipogenic ACE-PET/CT biomarkers in high-risk PC.

In study I and II, ACE-PET/CT showed an added diagnostic value in primary staging of high-risk PC, with higher detection rates of suspected LN metastases and bone metastases compared to standard methods clinical nomogram and BS. Also the result from study IV, with positive correlation between DIL and LN PET activity, supports that ACE-PET/CT is valid in N staging of high-risk PC.

These results add to patient benefit both in terms of patients being offered targeted curative treatment options, and in terms of avoiding inadequate or inappropriate therapy with possible negative effects on the quality of life. Both approaches would imply a reduction of adverse effects from therapies, by means of more accurate imaging-guided treatments.

The ideal endpoint for validation and assessment of the impact of ACE-PET/CT would be progression-free survival data. Second best would be histopathological confirmation of imaging findings, which could not be obtained in these studies since the patients were treated with radiotherapy. The best valuable comparator approach is a method that has

been validated in other comparative imaging studies in PC (95,96). The best valuable comparator, consisting of a consensus interpretation of all available information from PET/CT and other imaging findings and clinical follow-up, can be used as a substitute when histopathological confirmation is missing, to assess the performance of imaging methods. In study II, although for a limited number of patients, clinical follow-up consensus strongly supported ACE-PET/CT accuracy.
ACE-PET/CT had high impact (11-43%) on treatment strategy alterations, in agreement with previous reports from Kjölhede et al. on combined ^{18}F-choline-PET/CT and FDG-PET/CT (97), and from Lamanna et al. on ACE and ^{18}F-choline-PET (47). In addition, several studies on FDG-PET/CT in different cancers have shown a change in treatment plans ranging from 21-62%, due to PET/CT results (98–100).

The search for imaging biomarkers as prognostic tools is a hot topic in medical imaging today. In paper I, it was found that prostate $SUV_{max,DIL}$ might serve as a possible predictor of N+ disease in primary staging of high-risk PC. Paper IV aimed to further explore the associations between known clinical risk parameters and a number of ACE-PET/CT image metrics, to get a notion of the possible prognostic value of ACE-PET/CT. The previously found association between prostate lipogenic tumor burden and N+ disease on PET/CT was confirmed. No significant association was found between the established prognostic parameter nomogram risk and N+ disease, but nomogram risk was higher with higher prostate lipogenic tumor burden. These findings indicate that there may be an added prognostic value of ACE-PET/CT to the clinical nomogram in high-risk PC. To date, it is however premature to draw any

such definite conclusions from this result. Even high-risk PC requires long-term follow-up, minimum 36 months.

Except for the added diagnostic value of hybrid imaging, PET/CT also provides all N and M staging information in one procedure, consequently improving diagnostic work-up flow, and ultimately patient comfort. To optimize resource utilization of the PET/CT system, and to facilitate correct interpretation of findings, both the PET and the CT protocol should be tailored to perform at their best. In paper III, SharpIR 42% was recognized as the optimal method for PET reconstruction and thresholding in ACE-PET/CT, and this was further supported in paper IV. The added value of contrast-enhanced CT as part of the PET/CT protocol, has previously been shown for FDG-PET/CT (101). Compared to low-dose or diagnostic-dose non-contrast-enhanced CT, the contrast-enhanced CT provides improved morphological information regarding LNs, as well as visceral thoracic and abdominal processes. The interpretation of findings is based on the combined optimal information from PET and diagnostic-dose contrast-enhanced CT. An indisputable strength of the studies in this thesis is the hybrid imaging–hybrid reporting concept, as applied in clinical practice at the Nuclear Medicine section of Umeå University Hospital. Both PET and CT are performed with optimized protocols and the PET/CT examinations are subsequently read and reported in a standardized manner by two experienced physicians, double licensed in radiology and nuclear medicine. Another methodological strength is the homogeneity of the study participants fulfilling the inclusion criteria of the different studies. Most publications on ACE-PET/CT are in the recurrent setting. The studies in this thesis

add useful information to fill the knowledge gap regarding primary staging of previously untreated high-risk PC.

ACE-PET/CT in LN metastases

The mean observed proportion of N+ disease was higher than the mean nomogram risk. This result suggests that ACE-PET/CT may be superior to the clinical prediction nomogram. The possibility of clinical nomograms underestimating the risk of N+ disease has previously been discussed by Walz et al. (102). Another study showed that the specificity and accuracy of ^{11}C-choline-PET/CT in intermediate- and high-risk PC was better than that of clinical nomograms, although the results were not statistically significant (103).

On the other hand, the result of study I may reflect a high rate of false-positive findings. In that case, a possible cause for the discordance could be that the defined criteria for N+ disease were too generous.

LNs were reported as suspected metastases based on the combination of SUV_{max} and pre-defined morphological changes. However, pelvic LN appearance may be affected not only by PC-related metastatic growth, but also by reactive enlargement or by metastases from another synchronous cancer (104). Vice versa, normal-appearing LNs can contain micro-metastases. The optimal reference method would be histopathology with careful mapping of each ACE-avid LN, to get confirmation on lesion basis. For practical and ethical reasons, this is often difficult to achieve at surgery. At best, comparison is made by region-level. The patients in study I, II and IV were treated with radiotherapy, thus disabling the possibility of histopathological confirmation.

The frequently encountered low-grade ACE uptake in morphologically normal-appearing mediastinal LNs is considered non-specific, but the pathophysiological mechanism and any prognostic impact is unknown. Mediastinal lymphadenopathy in PC has been described in a number of case reports, and has been interpreted as a rare symptom of advanced disease (105–107). There is support for this manifestation of advanced PC in a post-mortem study on 176 patients, where the distribution of LN metastases from PC was most frequent in the paraaortal, external iliac and tracheobronchial regions (108). With more recent treatment options, this natural course of PC should be even less frequently encountered in medical imaging.

Altogether, the higher proportion of ACE-positive pelvic LNs found in study I is more likely representative of true LN metastases, while with current knowledge the interpretation of low-grade ACE uptake in morphologically normal-appearing mediastinal LNs remains non-metastatic.

$SUV_{max,DIL}$ was positively correlated to PSA and associated to N+ disease. The correlation between PSA and SUV was also shown in a recent study on ACE-PET/CT kinetics in low- and intermediate-risk PC (109), indicating the potential of prostate SUV as a biomarker for PC. The association between $SUV_{max,DIL}$ and N+ suggests that $SUV_{max,DIL}$ might be a possible predictor of pelvic LN metastases in primary staging of high-risk PC. The prognostic value of ACE-PET/CT image metrics is also supported by other studies as mentioned in the introduction (38).

ACE-PET/CT in bone metastases

The detection rate of suspected bone metastases was higher with ACE-PET/CT than with planar BS. Best valuable comparator, clinical follow-up consensus, from the majority of the discordant cases proved ACE-PET/CT correct, supporting the accuracy of ACE-PET/CT. The concordant ACE-PET/CT and BS cases were accepted as true positive and true negative without follow-up. These results comply well with the meta-analysis of BS, MRI and ^{11}C-choline-PET/CT in bone metastases in PC performed by Shen et al. (78), stating that BS was the least specific and least sensitive imaging method.

As a consequence of the 3-month time range allowed between ACE-PET/CT and BS, some metastases may have developed between the examinations. However, the 3-month time range has been established in other retrospective studies, and was considered reasonable as PC metastases are expected to exhibit a relatively slow growth rate (96).

ACE-PET/CT induced a change of therapy in 11% of the patients in paper II, due to previously undetected bone metastases or exclusion of bone metastases in patients with previously suspected but inconclusive findings in BS. This result is particularly remarkable in a study cohort with low pre-test probability of bone metastases. Despite the consecutive inclusion of eligible patients for the study, only those with a negative or inconclusive BS were referred for ACE-PET/CT according to clinical practice. With the retrospective design, patients with obvious bone metastases in BS were thus excluded from further diagnostic work-up with ACE-PET/CT, adding a selection bias to the study. This finding

further emphasizes the performance of ACE-PET/CT in detection of bone metastases.

Methodological improvements

SUV parameters were higher and volume parameters were lower with SharpIR than with VPHD reconstruction algorithm, as could be expected from the higher resolution with SharpIR compared to VPHD. The differences between SharpIR and VPHD were more accentuated with the 42% than with the estimated threshold. The least robust parameter was TLG, which can be understood from the formula for TLG, as the product of SUV_{mean} and FTV, where even small variations in SUV_{mean} and FTV will exert an influence on TLG.

SharpIR 42% showed the highest correlation with STV of LNs, in agreement with previous studies showing that fixed threshold values close to 42% reproduce reasonable estimates of true volumes in solid tumors with volumes >4 cm^3 and S/B-ratios >5.42 (88,89). The improved resolution achieved with SharpIR should explain why volume correlation with STV was better with SharpIR than with VPHD. Some LNs showed large discrepancies in STV and FTV. In general, FTV was smaller than STV in the larger LNs. This could be explained by only partial metastatic invasion of the LNs. In some smaller LNs, FTV was larger than STV, which may be interpreted as an artefact caused by limitations of the thresholding algorithm.

In the observed interval of 1 to 4 minutes, increasing acquisition time increased the volume parameters FTV and TLG, while SUV parameters were unaffected. Considering the desired amount of PET information and the feasible image acquisition time per examination, it is possible to

decrease image acquisition time to 2 minutes per bed position, with tolerable impairment of image quality.

An FDG-phantom developed for small volumes to simulate LNs, was used to further verify the optimal method for clinical ACE-PET/CT, SharpIR 42%. The FDG-phantom originated from another study (110) with the purpose to evaluate algorithms for volume delineation and partial volume correction in small volumes (< 0.7 ml). RCs for SUV_{max}, SUV_{mean} and one volume parameter, FTV, were considered sufficient, as TLG is derived from SUV_{mean} and FTV. The RCs for both SUV_{mean} and FTV improved with higher S/B ratio and larger balloon size. The problem with the underestimation of RC for SUV in small volumes is well known from studies of both PET and SPECT on the commercially available NEMA IEC Body Phantom (111).
The phantom measurements used in study III illustrate the relationship between lesion size, S/B-ratio and RC. If the lesion size and S/B-ratio are known, the true tumor SUV can be calculated from the measured SUV by means of RC. This could potentially be used in a future study to set up a clinical tool with RC-corrected SUV based on lesion size and S/B-ratio.

Prognostic potential of ACE-PET/CT

Inspired by the results from paper I, the aim of paper IV was to analyze associations between clinical risk parameters and lipogenic ACE-PET/CT biomarkers and thereby evaluate the possibility to use ACE-PET/CT in pre-therapeutic risk assessment of high-risk PC. Patients with N+ disease had higher prostate lipogenic tumor burden, measured in $SUV_{max,DIL}$ and TLU_{DIL}, thus supporting the association between

parameter $SUV_{max,DIL}$ and N+ disease previously found in paper I. It is likely that the parameter TLU_{DIL} represents a more robust and repeatable measurement than $SUV_{max,DIL}$, as TLU_{DIL} originates from $SUV_{mean,DIL}$ and is less susceptible to image noise. Altogheter, the result from study IV confirms the previous indication from study I, that lipogenic activity of the primary tumor in the prostate can serve as a predictor of N+ disease. Interestingly, despite the known problem of distinguishing the DIL from benign prostatic hyperplasia in ACE-PET/CT (86), the SUV_{max} and the lipogenic burden of the prostate thus appear to be important imaging biomarkers.

Nomogram risk correlated with TLU_{DIL}, but was not associated with N+ disease. It appears that the nomogram risk better reflects the prostate lipogenic tumor burden, than the actual LN parameters in ACE-PET/CT. This might be explained by the nomogram calculation which in part depends on primary tumor characteristics. Despite the lack of significant association between nomogram risk and N+ disease, the prostate lipogenic tumor burden in itself was linked to N+ disease. This discrepancy suggests an underestimation of LN risk by the clinical nomogram, as previously proposed in paper I. From a biological point of view it is reasonable to assume that more aggressive primary tumors tend to have a higher frequency of N+ disease. The significant correlation between ACE-PET activity in DIL and LNs further supports this argument.

The findings thus indicate that ACE-PET/CT biomarkers TLU_{DIL} and $SUV_{max,DIL}$ may have an added prognostic value compared to the clinical nomogram. Accordingly, a combination of the clinical nomogram and

ACE-PET/CT might provide a better, and in particular more individualized, risk assessment of LN metastases in high-risk PC.

The results of study IV are in line with Regula et al. (38), who suggested that total ACE uptake could serve as a biomarker for de novo malignant lipogenesis, which is linked to the aggressiveness of PC. In a recently published study by the same research group on ACE-PET/CT kinetics, intracellular ACE uptake rate (perfusion) and retention (anabolic metabolism) was increased in PC compared to normal tissue, suggesting that dynamic ACE-PET/CT could be used for monitoring PC aggressiveness and progression in low- and intermediate-risk PC (109). The implications of this perspective for high-risk PC remains to be investigated in future studies.
The results of study IV support the diagnostic value of ACE-PET/CT, and is also suggestive of the possible prognostic value. The currently presented data will be further evaluated with clinical endpoints biochemical relapse, time-to-progression and progression-free survival, at minimum follow-up of 36 months, and hopefully contribute to the knowledge regarding the added prognostic value of ACE-PET/CT compared to clinical risk parameters in primary staging of high-risk PC.

Limitations

The principal limitation of all the studies in this thesis is the lack of a reliable reference method. In paper I, the estimated nomogram risk was used as standard method, but the nomogram provides merely an estimated risk on group level. In paper II, BS served as standard method, but BS has a known specificity problem. In paper III, the standard

methods for validation were diagnostic contrast-enhanced CT and phantom FDG-PET. Thus, a different radiotracer than ACE was used for validation of ACE-PET reconstruction. For a correct comparison of CT lesion volume with FTV, the entire lesion volume must have undergone malignant transformation, which may not be the case in LNs. In paper IV, ACE-PET/CT parameters were compared with known clinical risk parameters, to identify possible lipogenic ACE-PET/CT biomarkers to be used for prognostic purposes. However, the prognostic impact of ACE-PET/CT can only be indirectly assumed from the associations between clinical risk parameters and lipogenic PET/CT parameters.

All the studies in this thesis suffer from statistical limitations pertaining to the small sample size. Therefore the results of the statistical analyses must be interpreted with care.

The two desired reference methods for the studies in this thesis are histopathological evaluation of ACE-PET/CT findings, and survival analyses, the latter of even more significant importance. Histopathology could not be obtained because the patients received radiotherapy. Survival analyses require long-term follow-up, and will be performed in future studies of the data from paper IV.

Conclusions

In primary staging of high-risk PC, ACE-PET/CT appears to have an added diagnostic value, with higher detection rates of suspected LN metastases and bone metastases compared to standard methods clinical nomogram and planar BS. ACE-PET/CT has a substantial impact on treatment strategy. PET reconstruction algorithm with resolution recovery and 42% fixed SUV threshold seems optimal for ACE-PET/CT.

Nomogram risk is associated with lipogenic tumor burden of the prostate, rather than to N+ disease on ACE-PET/CT. Lipogenic tumor burden of the prostate may act as a predictor of N+ disease on PET/CT.
Long-term prospective studies are needed to confirm the present data and to evaluate the prognostic impact of ACE-PET/CT in high-risk PC.

Acknowledgements

This research was funded by Umeå University, Västerbotten County Council (ALF) and Cancer Research Foundation Norrland.

I would like express my sincere gratitude to

Katrine Riklund, my main supervisor, who with great patience and wisdom has guided, supported and inspired me all along my clinical and academical development, and who first showed me the radiological light back in the days at medical school.

Camilla Thellenberg Karlsson, my assistant supervisor, who with enthusiasm and dedicated clinical knowledge has given me important insights into clinical practice, and who has provided the indispensable link between the patients and the research.

Jan Axelsson, my assistant supervisor, who with indefatigable commitment and support has spent innumerable hours helping me out with Excel sheets as well as radiophysics, and without whose careful proofreading no articles would ever have been finished.

Lennart Blomqvist, my assistant supervisor, both in person and on Skype, who has given me many a good advice on research, MRI and life.

Mattias and Margareta Ögren, our ambitious and curious radiochemists, without whose deep knowledge and spirit, ^{11}C-acetate production could not have been set up at Umeå University Hospital.

Anne Larsson Strömvall, for being ever so helpful with the details of gamma camera physics and image reconstruction.

Elin Wallsten and Jonas Andersson, for kindly adding to my limited knowledge of CT physics.

Hans Stenlund, who provided invaluable assistance in the statistical analyses, and also shared his knowledge and awakened my interest for statistics in several doctoral courses.

The patients who agreed to take part in this research, without whose kind consent none of this would have been possible.

Everyone at the Radiology department and especially at the Nuclear Medicine section, Umeå University Hospital, for being a part of our research-friendly clinic and for being such nice colleagues and friends.

Karin Berlin, for the artistic contribution to this thesis, with cover photo "The road forward, in hot iron color scale", symbolizing future PET research (in hot iron or other preferred color scale). From another aspect, the photo location on the Öland East coast is a link to my grandfather Ove, to whom this thesis is dedicated, and who spent many a summer holidays on Öland in his youth.

Last but not least, my wonderful family, by blood and by choice, I will always love you.

References

1. Prostate Cancer - Cancer Stat Facts [Internet]. [cited 2019 Dec 4]. Available from: https://seer.cancer.gov/statfacts/html/prost.html

2. Nationella prostatacancerregistret (NPCR) - RCC [Internet]. [cited 2020 Feb 23]. Available from: https://www.cancercentrum.se/samverkan/cancerdiagnoser/prostata/kvalitetsregister/

3. Zadra G, Photopoulos C, Loda M. The fat side of prostate cancer. Biochim Biophys Acta - Mol Cell Biol Lipids. 2013 Oct;1831(10):1518–32.

4. Rowley KHM, Mason MD. The aetiology and pathogenesis of prostate cancer. Clin Oncol. 1997 Jan 1;9(4):213–8.

5. Kessler B, Albertsen P. The natural history of prostate cancer. Urol Clin North Am. 2003;30(2):219–26.

6. Fonteyne V, Lumen N, Ost P, Van Praet C, Vandecasteele K, De Gersem Ir W, et al. Hypofractionated intensity-modulated arc therapy for lymph node metastasized prostate cancer: Early late toxicity and 3-year clinical outcome. Radiother Oncol. 2013;109(2):229–34.

7. Stephenson AJ, Kattan MW, Eastham JA, Dotan ZA, Bianco FJ, Lilja H, et al. Defining biochemical recurrence of prostate cancer after radical prostatectomy: A proposal for a standardized definition. J Clin Oncol. 2006;20(24):3973-8.

8. Budäus, L., Schiffmann, J., Graefen M et al. Defining biochemical recurrence after radical prostatectomy and timing of early salvage radiotherapy. Strahlenther Onkol. 2017;193(9):692–9.

9. Roach M, Hanks G, Thames H, Schellhammer P, Shipley WU, Sokol GH, et al. Defining biochemical failure following radiotherapy with or without hormonal therapy in men with clinically localized prostate cancer: Recommendations of the RTOG-ASTRO Phoenix Consensus Conference. Int J Radiat Oncol Biol Phys. 2006 Jul 15;65(4):965–74.

10. EAU Guidelines: Prostate Cancer | Uroweb [Internet]. [cited 2019 Dec 11]. Available from: https://uroweb.org/guideline/prostate-cancer/?type=summary-of-changes

11. Puente J, Grande E, Medina A, Maroto P, Lainez N, Arranz JA. Docetaxel in prostate cancer: a familiar face as the new standard in a hormone-

sensitive setting. Ther Adv Med Oncol. 2017 May;9(5):307–18.

12. Choi Y, Kim J, Kim N, Kim K, Choi E, Cho K. Functional MR Imaging of Prostate Cancer. Radiographics. 2007;(27):63–77.

13. Kendal WS, Mai KT. Histological subtypes of prostatic cancer: a comparative survival study. Can J Urol. 2010 Oct;17(5):5355–9.

14. Publications and Resources | UICC [Internet]. [cited 2019 Dec 11]. Available from: https://www.uicc.org/resources/tnm/publications-resources

15. Kane CJ, Eggener SE, Shindel AW, Andriole GL. Variability in Outcomes for Patients with Intermediate-risk Prostate Cancer (Gleason Score 7, International Society of Urological Pathology Gleason Group 2-3) and Implications for Risk Stratification: A Systematic Review. Eur Urol Focus. 2017 Oct 1;3(4–5):487–97.

16. Rodrigues G, Warde P, Pickles T, Crook J, Brundage M, Souhami L, et al. Pre-treatment risk stratification of prostate cancer patients: A critical review. Can Urol Assoc J. 2012;6(2):121–7.

17. Cagiannos I, Karakiewicz P, Eastham JA, Ohori M, Rabbani F, Gerigk C, et al. A preoperative nomogram identifying decreased risk of positive pelvic lymph nodes in patients with prostate cancer. J Urol. 2003;170(5):1798–803.

18. Bubendorf L, Schöpfer A, Wagner U, Sauter G, Moch H, Willi N, et al. Metastatic patterns of prostate cancer: An autopsy study of 1,589 patients. Hum Pathol. 2000;(31):578–83.

19. Maderthaner L, Furrer MA, Studer UE, Burkhard FC, Thalmann GN, Nguyen DP. More extended lymph node dissection template at radical prostatectomy detects metastases in the common iliac region and in the fossa of Marcille. BJU Int. 2018;121(5):725–31.

20. Nguyen DP, Huber PM, Metzger TA, Genitsch V, Schudel HH, Thalmann GN. A Specific Mapping Study Using Fluorescence Sentinel Lymph Node Detection in Patients with Intermediate- and High-risk Prostate Cancer Undergoing Extended Pelvic Lymph Node Dissection. Eur Urol. 2016;70(5):734–7.

21. Hensel J, Thalmann GN. Biology of Bone Metastases in Prostate Cancer. Urology. 2016 Jun;92:6–13.

22. Gandaglia G, Abdollah F, Schiffmann J, Trudeau V, Shariat SF, Kim SP, et al. Distribution of metastatic sites in patients with prostate cancer: A

population-based analysis. Prostate. 2014 Feb 1;74(2):210–6.

23. Hanahan D, Weinberg RA. The hallmarks of cancer. Cell. 2000 Jan 7;100(1):57–70.

24. Hanahan D, Weinberg RA. Hallmarks of Cancer: The Next Generation. Cell. 2011;144(5):646–74.

25. Kaplan RN, Riba RD, Zacharoulis S, Bramley AH, Vincent L, Costa C, et al. VEGFR1-positive haematopoietic bone marrow progenitors initiate the pre-metastatic niche. Nature. 2005 Dec 8;438(7069):820–7.

26. Hirakawa S. From tumor lymphangiogenesis to lymphvascular niche. Cancer Sci. 2009 Jun 1;100(6):983–9.

27. Velcheti V, Karnik S, Bardot SF, Prakash O. Pathogenesis of prostate cancer: lessons from basic research. Ochsner J. 2008;8(4):213–8.

28. Vāvere AL, Kridel SJ, Wheeler FB, Lewis JS. 1-11C-acetate as a PET radiopharmaceutical for imaging fatty acid synthase expression in prostate cancer. J Nucl Med. 2008;49(2):327–34.

29. Benedettini E, Nguyen P, Loda M. The pathogenesis of prostate cancer: from molecular to metabolic alterations. Diagn Histopathol (Oxf). 2008 May;14(5):195–201.

30. Suburu J, Chen YQ. Lipids and prostate cancer. Prostaglandins Other Lipid Mediat. 2012 May 1;98(1–2):1–10.

31. Mehralivand S, Shih JH, Harmon S, Smith C, Bloom J, Czarniecki M, et al. A Grading System for the Assessment of Risk of Extraprostatic Extension of Prostate Cancer at Multiparametric MRI. Radiology. 2019 Mar 22;290(3):709–19.

32. PI-RADS ® v2.1 PI-RADS ® Prostate Imaging-Reporting and Data System 2019 Version 2.1 PI-RADS ® Prostate Imaging-Reporting and Data System 2019 Version 2.1 ACKNOWLEDGEMENTS [Internet]. [cited 2020 Feb 18]. Available from: https://www.acr.org/-/media/ACR/Files/RADS/Pi-RADS/PIRADS-V2-1.pdf

33. Sherrer RL, Glaser ZA, Gordetsky JB, Nix JW, Porter KK, Rais-Bahrami S. Comparison of biparametric MRI to full multiparametric MRI for detection of clinically significant prostate cancer. Prostate Cancer Prostatic Dis. 2019 May 9;22(2):331–6.

34. Hövels AM, Heesakkers RAM, Adang EM, Jager GJ, Strum S, Hoogeveen YL, et al. The diagnostic accuracy of CT and MRI in the staging of pelvic

lymph nodes in patients with prostate cancer: a meta-analysis. Clin Radiol. 2008 Apr;63(4):387–95.

35. Even-Sapir E, Metser U, Mishani E, Lievshitz G, Lerman H, Leibovitch I. The detection of bone metastases in patients with high-risk prostate cancer: 99mTc-MDP Planar bone scintigraphy, single- and multi-field-of-view SPECT, 18F-fluoride PET, and 18F-fluoride PET/CT. J Nucl Med. 2006 Feb;47(2):287–97.

36. Wagenknecht G, Kaiser H-J, Mottaghy FM, Herzog H. MRI for attenuation correction in PET: methods and challenges. MAGMA. 2013;26(1):99.

37. Chen HH, Chiu NT, Su WC, Guo HR LB. Prognostic value of whole-body total lesion glycolysis at pretreatment FDG PET/CT in non-small cell lung cancer. Radiology. 2012;264(2):559–66.

38. Regula N, Häggman M, Johansson S, Sörensen J. Malignant lipogenesis defined by 11C-acetate PET/CT predicts prostate cancer-specific survival in patients with biochemical relapse after prostatectomy. Eur J Nucl Med Mol Imaging. 2016;43(12):2131–8.

39. Ona OH. Technescan™ HDP Kit for the Preparation of Technetium Tc 99m Oxidronate Rx only Diagnostic-For Intravenous Use [Internet]. [cited 2020 Feb 23]. Available from: https://www.accessdata.fda.gov/drugsatfda_docs/label/2017/018321s022lbl.pdf

40. Castellucci P, Jadvar H. PET/CT in prostate cancer: non-choline radiopharmaceuticals. Q J Nucl Med Mol imaging. 2012 Aug;56(4):367–74.

41. Jadvar H. Prostate cancer: PET with 18F-FDG, 18F- or 11C-acetate, and 18F- or 11C-choline. J Nucl Med. 2011;52(1):81–9.

42. Röthke MC, Afshar-Oromieh A, Schlemmer H-P. Potential of PET/MRI for diagnosis of prostate cancer. Radiologe. 2013;53(8):676–81.

43. Brogsitter C, Zöphel K, Kotzerke J. (18)F-Choline, (11)C-choline and (11)C-acetate PET/CT: comparative analysis for imaging prostate cancer patients. Eur J Nucl Med Mol Imaging. 2013;40(Suppl 1):18–27.

44. Bednarova S, Lindenberg ML, Vinsensia M, Zuiani C, Choyke PL, Turkbey B. Positron emission tomography (PET) in primary prostate cancer staging and risk assessment. Transl Androl Urol. 2017;6(3):413–23.

45. Schuster DM, Nanni C, Fanti S. PET Tracers Beyond FDG in Prostate Cancer. Semin Nucl Med. 2016;46(6):507–21.

46. Buchegger F, Garibotto V, Zilli T, Allainmat L, Jorcano S, Vees H, et al. First imaging results of an intraindividual comparison of (11)C-acetate and (18)F-fluorocholine PET/CT in patients with prostate cancer at early biochemical first or second relapse after prostatectomy or radiotherapy. Eur J Nucl Med Mol Imaging. 2013;41(1):68–78.

47. Lamanna G, Tabouret-Viaud C, Rager O, Jorcano S, Vees H-J, Seimbille Y, et al. Long-term Results of a Comparative PET/CT and PET/MRI Study of 11C-Acetate and 18F-Fluorocholine for Restaging of Early Recurrent Prostate Cancer. Clin Nucl Med. 2017;42(5):e242–6.

48. Picchio M, Berardi G, Fodor A, Busnardo E, Crivellaro C, Giovacchini G, et al. (11)C-Choline PET/CT as a guide to radiation treatment planning of lymph-node relapses in prostate cancer patients. Eur J Nucl Med Mol Imaging. 2014;41(7):1270–9.

49. Incerti E, Mapelli P, Gianolli L, Picchio M. PET imaging for lymph node dissection in prostate cancer. World J Urol. 2017;35(4):507–15.

50. Virgolini I, Decristoforo C, Haug A, Fanti S, Uprimny C. Current status of theranostics in prostate cancer. Eur J Nucl Med Mol Imaging. 2018;45(3):471–495.

51. Soloviev D, Fini A, Chierichetti F, Al-Nahhas A, Rubello D. PET imaging with 11C-acetate in prostate cancer: a biochemical, radiochemical and clinical perspective. Eur J Nucl Med Mol Imaging. 2008 May 13;35(5):942.

52. Schug ZT, Vande Voorde J, Gottlieb E. The metabolic fate of acetate in cancer. Nat Rev Cancer. 2016 Nov 26;16(11):708–17.

53. Madigan AA, Rycyna KJ, Parwani A V, Datiri YJ, Basudan AM, Sobek KM, et al. Novel nuclear localization of fatty acid synthase correlates with prostate cancer aggressiveness. Am J Pathol. 2014;184(8):2156–62.

54. Seltzer MA, Jahan SA, Sparks R, Stout DB, Satyamurthy N, Dahlbom M, et al. Radiation dose estimates in humans for (11)C-acetate whole-body PET. J Nucl Med. 2004;45(7):1233–6.

55. Nejabat M, Leisser A, Karanikas G, Wadsak W, Mitterhauser M, Mayerhöfer M, et al. [11C]acetate PET as a tool for diagnosis of liver steatosis. Abdom Radiol. 2018;43(11):2963–9.

56. Karanikas G, Beheshti M. ^{11}C-acetate PET/CT imaging: physiologic

uptake, variants, and pitfalls. PET Clin. 2014;9(3):339–44.

57. Tsuchiya J, Yamamoto M, Bae H, Oshima T, Yoneyama T, Miura O, et al. Tumor Identification of Less Aggressive or Indolent Lymphoma With Whole-Body 11C-Acetate PET/CT. Clin Nucl Med. 2019 Apr;44(4):276–81.

58. Grassi I, Nanni C, Allegri V, Morigi JJ, Montini GC, Castellucci P, et al. The clinical use of PET with (11)C-acetate. Am J Nucl Med Mol Imaging. 2012;2(1):33–47.

59. Liu RS. Clinical Application of [C-11]acetate in Oncology. Clin Positron Imaging. 2000;3(4):185.

60. Vardhanabhuti V, Lo AWI, Lee EYP, Law SYK. Dual-Tracer PET/CT Using 18F-FDG and 11C-Acetate in Gastric Adenocarcinoma With Liver Metastasis. Clin Nucl Med. 2016;41(11):864–5.

61. Zhu W, Dang Y, Ma Y, Li F, Huo L. 11C-Acetate PET/CT Monitoring Therapy of Multiple Myeloma. Clin Nucl Med. 2016;41(7):587–9.

62. Kim S, Kim D, Kim SH, Park M, Chang JH, Yun M. The roles of 11C-acetate PET/CT in predicting tumor differentiation and survival in patients with cerebral glioma. Eur J Nucl Med Mol Imaging. 2018 Jun 6;45(6):1012–20.

63. Klein LJ, Visser FC, Knaapen P, Peters JH, Teule GJ, Visser CA, et al. Carbon-11 acetate as a tracer of myocardial oxygen consumption. Eur J Nucl Med. 2001;28(5):651–68.

64. Araki T, Yoshida N, Tsuchiya T, Ikeda M, Namura M, Higuchi T, et al. Changes in myocardial oxidative metabolism after biventricular pacing as evaluated by [11C]acetate positron emission tomography. Ann Nucl Med. 2003;17(7):605–8.

65. Derlin T, Weiberg D, Sohns JM. Multitracer Molecular Imaging of Paget Disease Targeting Bone Remodeling, Fatty Acid Metabolism, and PSMA Expression on PET/CT. Clin Nucl Med. 2016;41(12):991–2.

66. Lindhe Ö, Sun A, Ulin J, Rahman O, Långström B, Sörensen J. [18F]Fluoroacetate is not a functional analogue of [11C]acetate in normal physiology. Eur J Nucl Med Mol Imaging. 2009;36(9):1453–9.

67. Oyama N, Akino H, Kanamaru H, Suzuki Y, Muramoto S, Yonekura Y, et al. 11C-Acetate PET Imaging of Prostate Cancer. J Nucl Med. 2002;43(2):181–6.

68. Czernin J, Benz MR, Allen-Auerbach MS. PET Imaging of Prostate Cancer Using C-Acetate. PET Clin. 2009;4(2):163–72.

69. Haseebuddin M, Dehdashti F, Siegel BA, Liu J, Roth EB, Nepple KG, et al. 11C-acetate PET/CT before radical prostatectomy: nodal staging and treatment failure prediction. J Nucl Med. 2013;54(5):699–706.

70. Mohsen B, Giorgio T, Rasoul ZS, Werner L, Ali GRM, Reza DKV, et al. Application of (11) C-acetate positron-emission tomography (PET) imaging in prostate cancer: systematic review and meta-analysis of the literature. BJU Int. 2013;(112):1062–72.

71. De Visschere PJL, Standaert C, Fütterer JJ, Villeirs GM, Panebianco V, Walz J, et al. A Systematic Review on the Role of Imaging in Early Recurrent Prostate Cancer. Eur Urol Oncol. 2019;2(1):47–76.

72. Almeida FD, Yen C-K, Scholz MC, Lam RY, Turner J, Bans LL, et al. Performance characteristics and relationship of PSA value/kinetics on carbon-11 acetate PET/CT imaging in biochemical relapse of prostate cancer. Am J Nucl Med Mol Imaging. 2017;7(1):1–11.

73. Daouacher G, von Below C, Gestblom C, Ahlström H, Grzegorek R, Wassberg C, et al. Laparoscopic extended pelvic lymph node (LN) dissection as validation of the performance of [11C]-acetate positron emission tomography/computer tomography in the detection of LN metastasis in intermediate- and high-risk prostate cancer. BJU Int. 2016;118(1):77–83.

74. Schumacher MC, Radecka E, Hellström M, Jacobsson H, Sundin A. [11 C]Acetate positron emission tomography-computed tomography imaging of prostate cancer lymph-node metastases correlated with histopathological findings after extended lymphadenectomy. Scand J Urol. 2015;49(1):35–42.

75. Esch LH, Fahlbusch M, Albers P, Hautzel H, Müller-Mattheis V. 11C-acetate positron-emission tomography/computed tomography imaging for detection of recurrent disease after radical prostatectomy or radiotherapy in patients with prostate cancer. BJU Int. 2017;120(3):337–42.

76. Huang S, Yin L, Yue J, Li Y, Yang Y, Lin Z. Direct comparison of choline PET/CT and MRI in the diagnosis of lymph node metastases in patients with prostate cancer. Medicine (Baltimore). 2018;97(50):e13344.

77. Polanec SH, Andrzejewski P, Baltzer PAT, Helbich TH, Stiglbauer A, Georg D, et al. Multiparametric [11C]Acetate positron emission tomography-magnetic resonance imaging in the assessment and staging of prostate cancer. PLoS One. 2017;12(7):e0180790.

78. Shen G, Deng H, Hu S, Jia Z. Comparison of choline-PET/CT, MRI, SPECT, and bone scintigraphy in the diagnosis of bone metastases in patients with prostate cancer: a meta-analysis. Skeletal Radiol. 2014;(43):1503–13.

79. Yu EY, Muzi M, Hackenbracht JA, Rezvani BB, Link JM, Montgomery RB, et al. C11-acetate and F-18 FDG PET for men with prostate cancer bone metastases: relative findings and response to therapy. Clin Nucl Med. 2011;36(3):192–8.

80. Giovacchini G, Incerti E, Mapelli P, Kirienko M, Briganti A, Gandaglia G, et al. [11C]Choline PET/CT predicts survival in hormone-naive prostate cancer patients with biochemical failure after radical prostatectomy. Eur J Nucl Med Mol Imaging. 2015;(42):877–84.

81. Tseng J-R, Yang L-Y, Lin Y-C, Liu C-Y, Pang S-T, Hong J-H, et al. Metabolic Volumetric Parameters in ^{11} C-Choline PET/MR Are Superior PET Imaging Biomarkers for Primary High-Risk Prostate Cancer. Contrast Media Mol Imaging. 2018 Nov 5;2018:1–10.

82. Farnebo J, Wadelius A, Sandström P, Nilsson S, Jacobsson H, Blomqvist L, et al. Progression-free and overall survival in metastatic castration-resistant prostate cancer treated with abiraterone acetate can be predicted with serial C11-acetate PET/CT. Medicine (Baltimore). 2016;95(31):e4308.

83. von Eyben FE, Kairemo K, Kiljunen T, Joensuu T. Planning of External Beam Radiotherapy for Prostate Cancer Guided by PET/CT. Curr Radiopharm. 2015;8(1):19–31.

84. Leisser A, Pruscha K, Ubl P, Wadsak W, Mayerhöfer M, Mitterhauser M, et al. Evaluation of fatty acid synthase in prostate cancer recurrence: SUV of [11 C]acetate PET as a prognostic marker. Prostate. 2015;75(15):1760–7.

85. von Below C, Wassberg C, Grzegorek R, Kullberg J, Gestblom C, Sörensen J, Waldén M AH. MRI and 11C Acetate PET/CT for Prediction of Regional Lymph Node Metastasis in Newly Diagnosed Prostate Cancer. Radiol Oncol. 2018;52(1):90–7.

86. Kato T, Tsukamoto E, Kuge Y, Takei T, Shiga T, Shinohara N, et al. Accumulation of [11C]acetate in normal prostate and benign prostatic hyperplasia: comparison with prostate cancer. Eur J Nucl Med Mol Imaging. 2002;29(11):1492–5.

87. Love C, Din AS, Tomas MB, Kalapparambath TP, Palestro CJ. Radionuclide Bone Imaging: An Illustrative Review. RadioGraphics. 2003;(23):341-58.

88. Boellaard R, O'Doherty MJ, Weber WA, Mottaghy FM, Lonsdale MN, Stroobants SG, et al. FDG PET and PET/CT: EANM procedure guidelines for tumour PET imaging: Version 1.0. Eur J Nucl Med Mol Imaging. 2010;(37):181–200.

89. Frings V, de Langen AJ, Smit EF, van Velden FHP, Hoekstra OS, van Tinteren H, et al. Repeatability of Metabolically Active Volume Measurements with 18F-FDG and 18F-FLT PET in Non-Small Cell Lung Cancer. J Nucl Med. 2010;(51):1870–1877.

90. Stroom J, Blaauwgeers H, van Baardwijk A, Boersma L, Lebesque J, Theuws J, et al. Feasibility of pathology-correlated lung imaging for accurate target definition of lung tumors. Int J Radiat Oncol Biol Phys. 2007;69(1):267–75.

91. Biehl KJ, Kong F-M, Dehdashti F, Jin J-Y, Mutic S, El Naqa I, et al. 18F-FDG PET Definition of Gross Tumor Volume for Radiotherapy of Non-Small Cell Lung Cancer: Is a Single Standardized Uptake Value Threshold Approach Appropriate? J Nucl Med. 2006;47(11):1808–12.

92. Strandberg S, Hashemi A, Axelsson J, Riklund K. Optimization of PET reconstruction algorithm, SUV thresholding algorithm and PET acquisition time in clinical 11C-acetate PET/CT. PLoS One. 2018 Dec 13;13(12):e0209169.

93. Liu D, Khong P-L, Gao Y, Mahmood U, Quinn B, St Germain J, et al. Radiation Dosimetry of Whole-Body Dual-Tracer 18F-FDG and 11C-Acetate PET/CT for Hepatocellular Carcinoma. J Nucl Med. 2016;57(6):907–12.

94. Bombardieri E, Giammarile F, Aktolun C, Baum RP, Bischof Delaloye A, Maffioli L, et al. Bone scintigraphy: procedure guidelines for tumour imaging. Eur J Nucl Med Mol Imaging. 2013;(30):99–106.

95. Lecouvet FE, El Mouedden J, Collette L, Coche E, Danse E JF et al. Can Whole-body Magnetic Resonance Imaging with Diffusion-weighted Imaging Replace Tc 99m Bone Scanning and Computed Tomography for Single-step Detection of Metastases in Patients with High-risk Prostate Cancer? Eur Urol. 2012 Jul 1;62(1):68–75.

96. Pyka T, Okamoto S, Dahlbender M, Tauber R, Retz M, Heck M, et al. Comparison of bone scintigraphy and68Ga-PSMA PET for skeletal staging in prostate cancer. Eur J Nucl Med Mol Imaging. 2016;43(12):2114–21.

97. Kjölhede H, Ahlgren G, Almquist H, Liedberg F, Lyttkens K, Ohlsson T, et al. Combined 18F-fluorocholine and 18F-fluoride positron emission tomography/computed tomography imaging for staging of high-risk

prostate cancer. BJU Int. 2012;110(10):1501–6.

98. Selzner M, Hany TF, Wildbrett P, McCormack L, Kadry Z, Clavien P-A. Does the novel PET/CT imaging modality impact on the treatment of patients with metastatic colorectal cancer of the liver? Ann Surg. 2004;240(6):1027–34.

99. Abdelmalik AG, Alenezi S, Muzaffar R, Osman MM. The Incremental Added Value of Including the Head in (18)F-FDG PET/CT Imaging for Cancer Patients. Front Oncol. 2013;3:71.

100. Tural D, Selcukbiricik F, Sager S, Akar E, Yildiz O, Serdengecti SH. PET-CT changes the management and improves outcome in patients with recurrent colorectal cancer. J Cancer Res Ther. 2014;10(1):121–6.

101. Houseni M, Osama A, Mohamed DI, Salem S. Value of contrast CT in combination with PET/CT in mesothelioma staging: Optimal protocol for initial assessment. Egypt J Radiol Nucl Med. 2017 Mar 1;48(1):67–74.

102. Walz J, Bladou F, Rousseau B, Laroche J, Salem N, Gravis G, et al. Head to head comparison of nomograms predicting probability of lymph node invasion of prostate cancer in patients undergoing extended pelvic lymph node dissection. Urology. 2012;79(3):546–51.

103. Schiavina R, Scattoni V, Castellucci P, Picchio M, Corti B, Briganti A, et al. 11C-choline positron emission tomography/computerized tomography for preoperative lymph-node staging in intermediate-risk and high-risk prostate cancer: comparison with clinical staging nomograms. Eur Urol. 2008;54(2):392–401.

104. Weingartner K, Ramaswamy A, Bittinger A, Gerharz EW, Voge D, Riedmiller H. Anatomical Basis for Pelvic Lymphadenectomy in Prostate Cancer: Results of an Autopsy Study and Implications for the Clinic. J Urol. 1996;156(6):1969–71.

105. Roca Edreira A, Aguilera Tubet C, Villanueva Peña A, Ballestero Diego R, Zubillaga Guerrero S. [Mediastinal lymph nodes during the course of a metastatic prostate cancer]. Actas Urol españolas. 2007;31(6):693–5.

106. Tsujino K, Sasada S, Kawahara K, Terada H, Komori C, Suzuki H, et al. [A case of prostatic adenocarcinoma clinically presenting as supraclavicular and mediastinal lymphadenopathy]. Nihon Kokyuki Gakkai Zasshi. 2007;45(8):648–53.

107. Perez NE, Maryala S, Seren S, Feng J, Pansare V, Dhar R. Metastatic prostate cancer presenting as mediastinal lymphadenopathy identified

by EUS with FNA. Gastrointest Endosc. 2007 May 1;65(6):948–9.

108. Arnheim FK. Carcinoma of the prostate; a study of the postmortem findings in 176 cases. J Urol. 1948 Oct;60(4):599–603.

109. Regula N, Honarvar H, Lubberink M, Jorulf H, Ladjevardi S, Häggman M, et al. Carbon Flux as a Measure of Prostate Cancer Aggressiveness: [^{11} C]-Acetate PET/CT. Int J Med Sci. 2020;17(2):214–23.

110. Wallsten E, Axelsson J, Sundstrom T, Riklund K, Larsson A. Subcentimeter Tumor Lesion Delineation for High-Resolution 18F-FDG PET Images: Optimizing Correction for Partial-Volume Effects. J Nucl Med Technol. 2013 Jun 1;41(2):85–91.

111. Jönsson L, Stenvall A, Mattsson E, Larsson E, Sundlöv A, Ohlsson T, et al. Quantitative analysis of phantom studies of 111In and 68Ga imaging of neuroendocrine tumours. EJNMMI Phys. 2018 Feb 20;5(1):5.